

Changes in apparent temperature and PM_{2.5} around the Beijing-Tianjin megalopolis under greenhouse gas and stratospheric aerosol ~~injection~~ intervention scenarios

Jun Wang¹, John C. Moore^{1,2*}, Liyun Zhao^{1*}

¹College of Global Change and Earth Systems Science, Beijing Normal University, Beijing 100875, China

²Arctic Center, University of Lapland, Rovaniemi, Finland

Correspondence to: zhaoliyun@bnu.edu.cn, john.moore.bnu@gmail.com

Abstract. Apparent temperatures (AP) and ground level aerosol pollution (PM_{2.5}) are important factors in human health, particularly in rapidly growing urban centres in the developing world. We quantify how changes in apparent temperature – that is a combination of 2 m air temperature, relative humidity and surface wind speed, and PM_{2.5} concentrations – that depend on the same meteorological factors along with future industrial emission policy, may impact people in the greater Beijing region. Four Earth System Models (ESM) simulations of the modest greenhouse emissions RCP4.5, the “business-as-usual” RCP8.5 and the stratospheric aerosol ~~injection~~ intervention G4 geoengineering scenarios are downscaled using both a 10 km resolution dynamic model (WRF), and a statistically approach (ISIMIP). We use multiple linear regression models to simulate changes in PM_{2.5} and the contributions meteorological factors make in controlling seasonal AP and PM_{2.5}. WRF produces warmer winters and cooler summers than does ISIMIP both now and in the future. These differences mean that estimates of numbers of days with extreme apparent temperatures vary systematically with downscaling method, as well as between climate models and scenarios. Air temperature changes dominate differences in apparent temperatures between future scenarios even more than they do at present because the reductions in humidity expected under solar geoengineering are overwhelmed by rising vapor pressure due to rising temperatures and the lower windspeeds expected in the region in all future scenarios. Compared with the 2010s, PM_{2.5} concentration is projected to decrease 5.4 µg/m³ in the Beijing-Tianjin province under the G4 scenario during the 2060s from the WRF downscaling, but decrease by 7.6 µg/m³ using ISIMIP. The relative risk of 5 diseases decreases by 1.1%-6.7% in G4/RCP4.5/RCP8.5 using ISIMIP, but have smaller decrease (0.7%-5.2%) using WRF. Temperature and humidity differences between scenarios change the relative risk of disease from PM_{2.5} such that G4 results in 1-3% higher health risks than RCP4.5. Urban centres see larger rises in extreme apparent temperatures than rural surroundings due to differences in land surface type, and since these are also the most densely populated, health impacts will be dominated by the larger rises in apparent temperatures in these urban areas.

41 **500 character non-technical text**

42 Apparent temperatures and PM_{2.5} pollution depends on humidity and wind speed in
43 addition to surface temperature and impacts human health and comfort. Apparent
44 temperatures will reach dangerous levels more commonly in future because of water
45 vapor pressure rises and lower expected wind speeds, but these will also drive change
46 in PM_{2.5}. Solar geoengineering can reduce the frequency of extreme events significantly
47 relative to modest, and especially “business as usual” greenhouse scenarios.

48
49
50 **1. Introduction**

51 Global mean surface temperature has increased by 0.92°C (0.68-1.17°C) during 1880-
52 2012 (IPCC, 2021), which naturally also impacts the human living environment
53 (Kraaijenbrink et al., 2017; Garcia et al., 2018). However, neither land surface
54 temperature nor near-surface air temperature can adequately represent the temperature
55 we experience. Apparent temperature (AP), that is how the temperature feels, is
56 formulated to reflect human thermal comfort and is probably a more important
57 indication of health than daily maximum or minimum temperatures (Fischer et al., 2013;
58 Matthews et al., 2017; Wang et al., 2021). There are various approaches to estimating
59 how the weather conditions affect comfort, but apparent temperature is governed by air
60 temperature, humidity and wind speed (Steadman 1984; Steadman 1994). These are
61 known empirically to affect human thermal comfort (Jacobs et al., 2013), and thresholds
62 have been designed to indicate danger and health risks under extreme heat events (Ho
63 et al., 2016). Analysis of historical apparent temperatures in China (Wu et al., 2017; Chi
64 et al., 2018; Wang et al., 2019), Australia (Jacobs et al., 2013), and the USA (Grundstein
65 et al., 2011) all find that apparent temperature is increasing faster than air temperature.
66 This is due to both decreasing wind speeds and, especially to increasing vapor pressure
67 (Song et al., 2022).

68
69 As the world warms, apparent temperature is expected to rise faster than air
70 temperatures in the future (Li et al., 2018; Song et al., 2022). Hence, humans, and other
71 species, will face more heat-related stress but less cold-related environmental stress in
72 the warmer future (Wang et al., 2018; Zhu et al., 2019). Since most of the population is
73 now urban, the conditions in cities will determine how tolerable are future climates for
74 much of humanity, while the differences in thermal comfort between urbanized and
75 rural regions will be a factor in driving urbanization. Reliable estimates of future urban
76 temperatures and their rural surroundings require methods to improve on standard
77 climate model resolution to adequately represent the different land surface types;
78 especially the rapid and accelerating changes in land cover in the huge urban areas
79 characteristic of sprawling developments in the developing world. This is usually done
80 with either statistical or dynamic downscaling approaches, and in this article we
81 examine both methods.

82

83 In early 2013, Beijing encountered a serious pollution incident. The concentration of
84 PM_{2.5} (particles with diameters less than or equal to 2.5 μm in the atmosphere) exceeded
85 500 μg/m³ (Wang et al., 2014). Following this event and its expected impacts on human
86 health (Guan et al., 2016; Fan et al., 2021) and the economy (Maji et al., 2018; Wang
87 et al., 2020), the Beijing municipal government launched the Clean Air Action Plan in
88 2013. The annual mean concentration of PM_{2.5} in Beijing-Tianjin-Hebei region
89 decreased from 90.6 μg/m³ in 2013 to 56.3 μg/m³ in 2017, a decrease of about 38%
90 (Zhang et al., 2019), although this is still more than double the EU air quality standard
91 (25 μg/m³) and above the Chinese FGNS (First Grand National Standard) of 35 μg/m³.
92 The concentration of PM_{2.5} is related to anthropogenic emissions, but also dependent
93 on meteorological conditions (Chen et al., 2020). Simulations suggested that 80% of
94 the 2013-2017 lowering of PM_{2.5} concentration came from emission reductions in
95 Beijing (Chen et al. 2019). Humidity and temperature are the main meteorological
96 factors affecting PM_{2.5} concentration in Beijing in summer, while humidity and wind
97 speed are the main factors in winter (Chen et al., 2018). Simulations driven by different
98 RCP emission scenarios with fixed meteorology for the year 2010 suggest that PM_{2.5}
99 concentration will meet FGNS under RCP2.6, RCP4.5 and RCP8.5 in Beijing-Tianjin-
100 Hebei after 2040 (Li et al., 2016).

101

102 The focus here is in the differences in apparent temperature and PM_{2.5} that may arise
103 from solar geoengineering (that is reduction in incoming short-wave radiation to offset
104 longwave absorption by greenhouse gases) via stratospheric aerosol ~~injection~~
105 inervention (SAI), and pure greenhouse gas climates. We use all four climate models
106 that have provided sufficient data from the G4 scenario described by the
107 Geoengineering Model Intercomparison Project (GeoMIP). G4 specifies sulfates as the
108 aerosol, and greenhouse gas emissions from the RCP4.5 scenario (Kravitz et al., 2011).
109 The impacts of G4 on surface temperature and precipitation have been discussed at
110 regional scales (Yu et al., 2015) and both are lowered relative to RCP4.5. Some studies
111 have focused on regional impact of SAI on apparent or wet bulb temperatures: in
112 Europe, (Jones et al., 2018); East Asia (Kim et al., 2020); and the Maritime Continent
113 (Kuswanto et al., 2021). But none of these studies have considered apparent
114 temperature at scales appropriate for rapidly urbanizing regions such as on the North
115 China Plain. The only study to date on SAI impacts on PM_{2.5} pollution was a coarse
116 resolution (4°×5°) global scale model with sophisticated chemistry (Eastham et al.,
117 2018). They simulated aerosol rainout from the stratosphere to ground level, leading to
118 an eventual increase in ground level PM_{2.5}. Eastham et al. (2018) concluded that SAI
119 changes in tropospheric and stratospheric ozone dominated PM_{2.5} impacts on global
120 mortality. However, this study included only a first-order estimate of temperature and
121 precipitation change on PM_{2.5} concentration under geoengineering, and also did not
122 consider ~~meteorological effects nor~~ the situation in a highly polluted urban environment
123 such as included in our domain, and which is typical of much of the developing world.

124

125 The greater Beijing megalopolis lies in complex terrain, surrounded by hills and

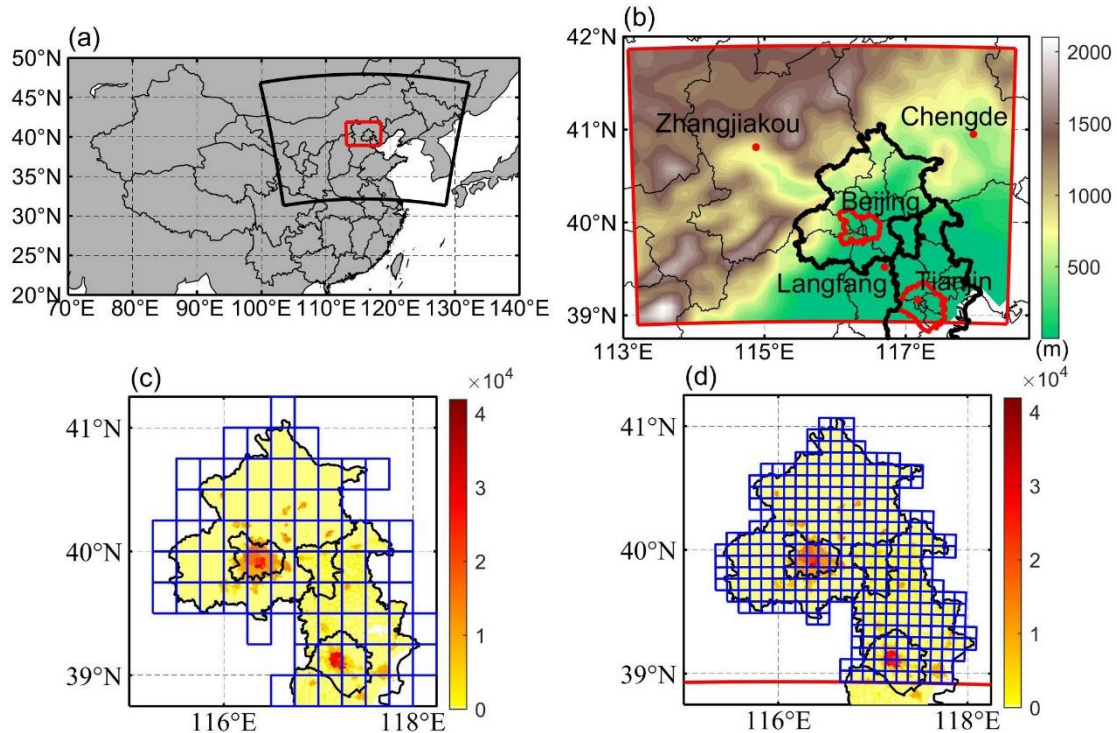
126 mountains on three sides, and a flat plain to the southeast coast (Fig. 1). Over the period
127 1971-2014, apparent temperature rose at a rate of $0.42^{\circ}\text{C}/10$ years over Beijing-Tianjin-
128 Hebei region, with urbanization having an effect of $0.12^{\circ}\text{C}/10$ years (Luo and Lau,
129 2021). By the end of 2019, the permanent resident population in Beijing exceeded 21
130 million. Tianjin, 100 km from Beijing, is the fourth largest city in China with a
131 population of about 15 million, and Langfang (population 4 million) is about 50 km
132 from Beijing. Thus, the region contains a comparable urbanized population as the
133 northeast US megalopolis. Since its climate is characterized by hot and moist summer
134 monsoon conditions, the population is at an enhanced risk as urban heat island effects
135 lead to city temperatures warming faster than their rural counterparts.

136

137 There are large uncertainties in projecting $\text{PM}_{2.5}$ concentration in the future due to both
138 climate and industrial policies. Statistical methods are much faster than atmospheric
139 chemistry models (Mishra et al., 2015), and different scenarios are easy to implement.
140 We use a Multiple Linear Regression (MLR) model to establish the links between $\text{PM}_{2.5}$
141 concentration, meteorology and emissions (Upadhyay et al., 2018; Tong et al., 2018).
142 We project and compare the differences of $\text{PM}_{2.5}$ concentration under G4 and RCP4.5
143 scenarios, and between different $\text{PM}_{2.5}$ emission scenarios. Accurate meteorological
144 data are crucial in simulating future apparent temperatures and $\text{PM}_{2.5}$ because all ESM
145 suffer from bias, and this problem is especially egregious at small scales. A companion
146 paper (Wang et al., 2022) looked at differences between downscaling methods with the
147 same 4 Earth System Models (ESM), domain and scenarios as we use here.

148

149 In this paper, we use the downscaled data to explore the effect of SAI on apparent
150 temperature and $\text{PM}_{2.5}$ over the greater Beijing megalopolis. The paper is organized as
151 follows. The data and methods of calculating AP, AP thresholds, the $\text{PM}_{2.5}$ MLR model
152 and its validation are briefly described in Section 2. The results from present day
153 simulation and future projections on apparent temperature and $\text{PM}_{2.5}$ are given in
154 Section 3, along with their associated impact analyses. In Section 4 we discuss and
155 interpret the findings, and finally we conclude with a summary of the main implications
156 of the geoengineering impacts on these two important human health indices in Section
157 5.



158 **Figure 1.** **a**, The 10 km WRF domain (red box) nested inside a 30 km resolution WRF domain (large
 159 black sector). **b**, The inner domain topography and major conurbations (red dots), with the urban areas
 160 of Beijing and Tianjin enclosed in red curves. Panels **c** and **d** show the population density (persons per
 161 km²) of Beijing and Tianjin provinces (defined by black borders) in 2010 and the grid cells within the
 162 Beijing-Tianjin province (blue boxes) when downscaled by ISIMIP (**c**) and WRF (**d**).
 163

164 2. Data and Methods

165 2.1 Scenarios, ESM, downscaling methods and bias correction

166 The scenarios, ESM, downscaling methods and bias correction methods we use here
 167 are as described in detail by Wang et al., (2022), and we just summarize the method
 168 briefly here. We use three different scenarios: RCP4.5 and RCP8.5 (Riahi et al., 2011)
 169 and the GeoMIP G4 scenario which span a useful range of climate scenarios: RCP4.5
 170 is similar (Vandyck et al., 2016) to the expected trajectory of emissions under the 2015
 171 Paris Climate Accord agreed Nationally Determined Contributions (NDCs); RCP8.5
 172 represents a formerly business-as-usual, no climate mitigation policies, large signal to
 173 noise ratio scenario; G4 represents a similar radiative forcing as produced by the 1991
 174 Mount Pinatubo volcanic eruption repeating every 4 years.

175
 176 Climate simulations are performed by 4 ESM: BNU-ESM (Ji et al., 2014), HadGEM2-
 177 ES (Collins et al., 2011), MIROC-ESM (Watanabe et al., 2011) and MIROC-ESM-
 178 CHEM (Watanabe et al., 2011). We compare dynamical and statistical downscaling
 179 methods to convert the ESM data to scales more suited to capturing differences between
 180 contrasting rural and urban environments. To validate the downscaled AP from model
 181 results, we use the daily temperature, humidity and wind speed during 2008-2017 from
 182 the gridded observational dataset CN05.1 with the resolution of $0.25^{\circ} \times 0.25^{\circ}$ based on

183 the observational data from more than 2400 surface meteorological stations in China,
184 which are interpolated using the “anomaly approach” (Wu and Gao, 2013). This dataset
185 is widely used, and has good performance relative to other reanalysis datasets over
186 China (Zhou et al., 2016; Yang et al., 2019; Yang et al., 2023; Yang and Tang, 2023).
187 Dynamical downscaling for the 4 ESM datasets was done with WRFv.3.9.1 with a
188 parameter set used for urban China studies (Wang et al., 2012) in two nested domains
189 at 30 and 10 km resolution over 2 time slices (2008-2017 and 2060-2069). We corrected
190 the biases in WRF output using the quantile delta mapping method (QDM; Wilcke et
191 al., 2013) with ERA5 (Hersbach et al., 2018) to preserve the mean probability density
192 function of the output over the domain without degrading the WRF spatial pattern. All
193 WRF results presented are after QDM bias correction. Statistical downscaling was done
194 with the trend-preserving statistical bias-correction Inter-Sectoral Impact Model
195 Intercomparison Project (ISIMIP) method (Hempel et al., 2013) for the raw ESM output,
196 producing output matching the mean ERA5 observational data in the reference
197 historical period with the same spatial resolution, while allowing the individual ESM
198 trends in each variable to be preserved.

199

200 **2.2 PM_{2.5} concentration and emission data**

201 In China there were few PM_{2.5} monitoring stations before 2013 (Xue et al., 2021).
202 However, aerosol optical depths produced by the Moderate Resolution Imaging
203 Spectroradiometer (MODIS) have been used to build a daily PM_{2.5} concentration
204 dataset (ChinaHighPM2.5) at 1 km resolution from 2000 to 2018 (Wei et al., 2020). We
205 use monthly PM_{2.5} concentration data during 2008-2015 from ChinaHighPM2.5 to train
206 the MLR model, and the data during 2016-2017 to validate it. Figure S1 shows annual
207 PM_{2.5} concentration over Beijing areas during 2008 (a) and 2017 (b).

208

209 Recent gridded monthly PM_{2.5} emission data were derived from the Hemispheric
210 Transport of Air Pollution (HTAP_V3) with a resolution of 0.1°×0.1° during 2008-2017,
211 which is a widely used anthropogenic emission dataset (Janssens-Maenhout et al.,
212 2015). PM_{2.5} emissions over Beijing areas during 2008 (c) and 2017 (d) are shown in
213 Fig. S1.

214

215 Future gridded monthly PM_{2.5} emissions to 2050 are available in the ECLIPSE V6b
216 database (Stohl et al., 2015), generated by the GAINS (Greenhouse gas Air pollution
217 Interactions and Synergies) model (Klimont et al., 2017). The ECLIPSE V6b baseline
218 emission scenario assumes that future anthropogenic emissions are consistent with
219 those under current environmental policies, hence it is the “worst” scenario without
220 considering any mitigation measures (Li et al., 2018; Nguyen et al., 2020). Projected
221 emissions are shown in Fig S2, with emissions plateauing at ~40 kt/year after 2030, so
222 we assume 2060s levels are similar. These ECLIPSE projections are significantly larger
223 than present day estimates from HTAP_V3. We therefore estimate 2060s emissions as
224 the recent gridded monthly PM_{2.5} emissions from HTAP_V3 scaled by the ratios of
225 2050 ECLIPSE emission to average annual emissions between 2010 and 2015. Before

226 processing data, PM_{2.5} concentration is bilinearly interpolated to the WRF and ISIMIP
227 grids, while PM_{2.5} emissions are conservatively interpolated to the target grids.
228

229 2.3 Apparent temperature

230 We used ~~the a widely used empirical formula formula proposed in Steadman (1984)~~ to
231 ~~estimate calculate the~~ apparent temperature under shade (Steadman 1984), ~~that~~
232 ~~combines various meteorological fields,~~ which ~~also~~ has been widely used to study heat
233 waves, heat stress and temperature-related mortality (Perkins and Alexander, 2013;
234 Lyon and Barnston, 2017; Lee and Sheridan, 2018; Zhu et al., 2021):

$$235 AP = -2.7 + 1.04 \times T + 2 \times P - 0.65 \times W \quad (1)$$

236 where AP is the apparent temperature (°C) under shade meaning that radiation is not
237 considered; T is the 2 m temperature (°C), W is the wind speed at 10 m above the ground
238 (m/s), and P is the vapor pressure (kPa) calculated by

$$239 P = P_s \times RH \quad (2)$$

240 where P_s is the saturation vapor pressure (kPa), and RH is the relative humidity (%).
241 P_s is calculated using the Tetens empirical formula (Murray, 1966):

$$242 P_s = \begin{cases} 0.61078 \times e^{\left(\frac{17.2693882 \times T}{T+237.3}\right)}, & T \geq 0 \\ 0.61078 \times e^{\left(\frac{21.8745584 \times (T-3)}{T+265.5}\right)}, & T < 0 \end{cases} \quad (3)$$

243 To assess the potential risks of heat-related exposure from apparent temperature, we
244 also count the number of days with $AP > 32^\circ\text{C}$ (NdAP_32) in the Beijing-Tianjin
245 province (Table S1). This threshold does not lead to extreme risk and death, instead it
246 is classified as requiring “extreme caution” by the US National Weather Service
247 (National Weather Service Weather Forecast Office,
248 <https://www.weather.gov/ama/heatindex>), but carries risks of heatstroke, cramps and
249 exhaustion. A threshold of 39°C is classed as “dangerous” and risks heatstroke. While
250 hotter AP thresholds would give a more direct estimate of health risks, the statistics of
251 these presently rare events mean that detecting differences between scenarios is less
252 reliable than using the cooler NdAP_32 threshold simply because the likelihood of rare
253 events are more difficult to accurately quantify than more common events that are
254 sampled more frequently. There is evidence that in some distributions, the likelihood
255 of extremes will increase more rapidly than central parts of a probability distribution,
256 for example large Atlantic hurricanes increasing faster than smaller ones (Grinsted et
257 al., 2013). But the conservative assumption is that similar differences between scenarios
258 would apply for higher thresholds as lower ones.

259 2.4 Population Data Set

260 Since health impacts ~~are more important where there are more people~~ scale with the
261 number of people affected, we calculate the NdAP_32 weighted by population (Fig. 1c
262 and 1d). We employ gridded population data (Fu et al., 2014;
263 <https://doi.org/10.3974/geodb.2014.01.06.V1>) with a spatial resolution of 1×1 km
264 collected in 2010. The population density distribution in Beijing and Tianjin provinces
265 with the ISIMIP and WRF grid cells contained are shown in the Fig. 1c and 1d.

266

267 2.5 MLR model calibration

268 Many meteorological factors, such as temperature (You et al., 2017), precipitation (Guo
269 et al., 2016), wind speed (Yin et al., 2017), radiation (Chen et al., 2017), planetary
270 boundary layer height (Zheng et al., 2017) etc., can affect the PM_{2.5} concentration. Their
271 relative importance differs regionally. But here we consider only differences that are
272 produced by the three scenarios, so for example we do not include precipitation in our
273 analysis because none of the ESM simulate significant changes in our domain (Table
274 S2). Previous studies have shown that wind and humidity are the dominant
275 meteorological variables for PM_{2.5} concentration in region we study (Chen et al., 2020),
276 while changes in temperature and winds obviously impact local concentrations. Hence,
277 we generate an MLR model between PM_{2.5} and temperature (T), relative humidity (H),
278 zonal wind (U), meridional wind (V) and PM_{2.5} emissions (E) at every grid cell as
279 follows:

280

$$281 \quad PM_{2.5} = \sum a_i X_i + b \quad (4)$$

282 Where $X_{i(i=1,2,3,4,5)}$ are the five factors, a_i are the regression coefficients of the X_i
283 with $PM_{2.5}$, and b is the intercept, which is a constant. We assume that all factors
284 should be included in the regression. All the meteorological variables are from the
285 statistical and dynamical downscaling and bias corrected results during 2008-2017,
286 with the first 8 years used for training model and the second 2 years used for validating
287 model. We train the MLR for the 4 ESMs under statistical and dynamical downscaling
288 in each grid cell separately, thus accounting spatial differences in the weighting of the
289 X_i across the domain. Meteorological variables under G4, RCP4.5 and RCP8.5 during
290 2060-2069 are used for projection.

291

292 Here, we use PM_{2.5} concentration including both primary and secondary PM_{2.5} as the
293 dependent variable and primary PM_{2.5} emission and meteorological factors as
294 independent variables in the MLR. Future PM_{2.5} emissions will change in ways that are
295 rather speculative as they depend on technological innovation and policies that are
296 inherently unpredictable. The MLR assumes that the past emissions mix and secondary
297 aerosols remain unchanged in the future, but meteorological factors will also indirectly
298 impact secondary PM_{2.5} to some extent.

299

300 The contributions of meteorology and PM_{2.5} emissions on future concentrations are
301 examined by using recent PM_{2.5} emissions (baseline) and future PM_{2.5} emissions
302 (mitigation), and the downscaled climate scenarios. Modeled PM_{2.5} concentration using
303 recent meteorology and PM_{2.5} emissions during 2008-2017 (2010s) is considered as our
304 reference.

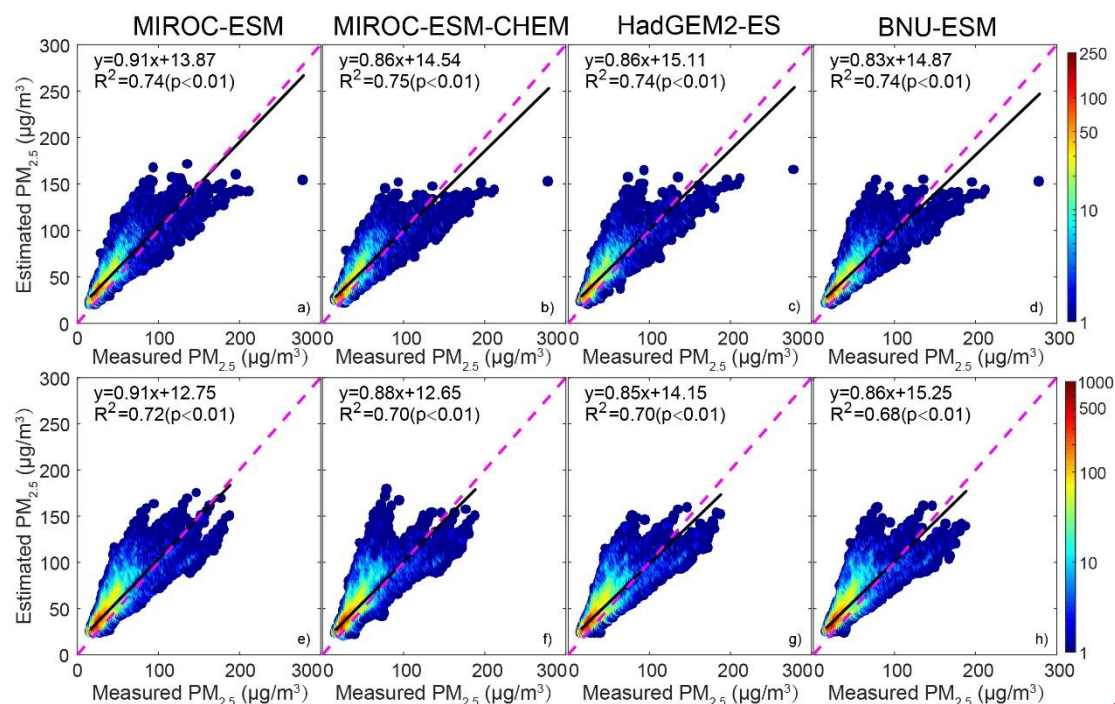
305

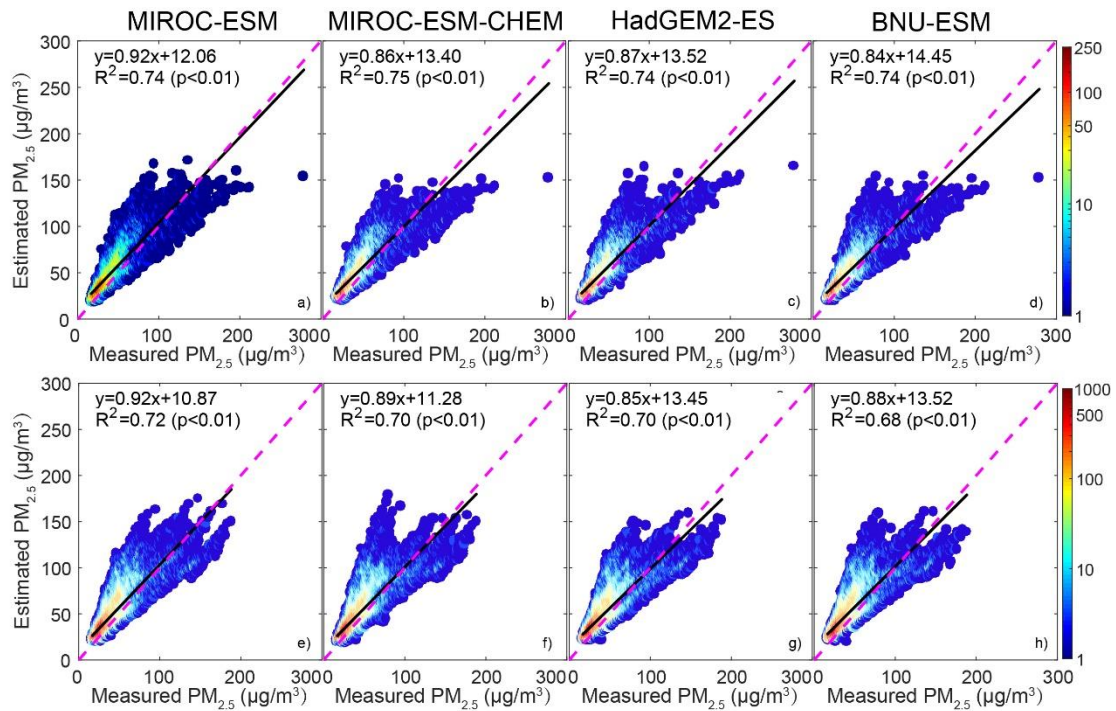
306 Collinearity of variables is inevitable in our domain. The domination of the seasonal
307 winter and summer monsoonal weather patterns mean that temperatures, precipitation

308 and wind direction are all highly seasonal and correlated. In winter, precipitation is
 309 minimal and northerly winds predominate, in summer the opposite is true. These three
 310 meteorological fields are important and also important for emissions, since sources are
 311 essentially absent from the north, while temperature and humidity dominate aerosol
 312 microphysics.

313
 314 We use the variance inflation factor (VIF) to test if there is excessive collinearity in our
 315 MLR models. Generally, if VIF value is greater than 10, there is collinearity problem
 316 between variables. Figure S3 shows that there are indeed collinearity problems in some
 317 areas, but not in Beijing-Tianjin province, so there is no impact on the results for the
 318 urban areas. We explored the impact of collinearity on the results in high VIF grid cells
 319 by removing factors with VIF greater than 10 and the full variables model (Fig. S4 and
 320 Fig. S5). Using ISIMIP downscaling, we only removed the temperature, while we
 321 removed the temperature and U-wind in the WRF method. PM_{2.5} concentrations
 322 increased by ~1 μg/m² in all ESMs under G4 with the “baseline” scenario (Fig. S4), in
 323 contrast, PM_{2.5} concentrations decreased by 5-15 μg/m² with the “mitigation” scenario
 324 (Fig. S5) after dealing the collinearity problem. This means that PM_{2.5} concentration
 325 has more sensitivity to the PM_{2.5} emission after accounting for collinearity. Although
 326 the absolute PM_{2.5} concentrations are different accounting for collinearity, there are no
 327 significant differences in the changes of PM_{2.5} concentration between G4 and the
 328 2010s/RCP4.5/RCP8.5 in Beijing-Tianjin province.

329 2.6 MLR model validation





331

332 **Figure 2.** Scatter-grams of PM_{2.5} concentration derived by MODIS and estimated by MLR during
 333 validation period (2016-2017). Top figures (a-d) are the ISIMIP statistical downscaling results, and
 334 bottom figures (e-h) are the WRF dynamical downscaling results. R² means the variance explained
 335 by the MLR, and color bar denotes the density of datapoints at integer intervals.

336

337 Figure 2 shows the scattergram of PM_{2.5} concentration between ChinaHighPM2.5
 338 dataset and MLR model during validation period based on ISIMIP and WRF results.
 339 Observations and MLR models have Pearson's correlations coefficients around 0.86 for
 340 ISIMIP results during the validation period, and the coefficient of determination of
 341 MLRs are 0.74-0.75 (Fig. 2a-d). WRF Pearson's correlations are slightly lower, 0.82-
 342 0.85, and explained variance ranges from 0.68-0.72 (Fig. 2e-h). These results are
 343 similar as found by Jin et al. (2022). We also compare the spatial patterns of observed
 344 and modeled PM_{2.5} in Fig. S3S6. Both ISIMIP and WRF results can simulate the
 345 distribution characteristics of high concentration of PM_{2.5} in the southeast and low
 346 concentration in the northwest.

347

348 We also tested the accuracy of our MLR model projection against simulations (Li et al.,
 349 2023) with the Community Multiscale Air Quality (CMAQ) model developed by the
 350 United States Environmental Protection Agency and which can simulate particulate
 351 matter on local scales (Foley et al., 2010; Yang et al., 2019) when coupled to WRF. We
 352 used the same meteorological forcing as Li with the "EIT1" PM_{2.5} emissions scenario
 353 in 2050 under RCP4.5 (Fig.S7). The spatial patterns are well correlated in all seasons
 354 (0.68-0.73), but PM_{2.5} concentrations are about twice as high in our MLR model as
 355 from Li et al., (2023). PM_{2.5} concentrations from our regression model are also higher
 356 than the referenced data during 2008-2017. While the difference in absolute PM_{2.5}
 357 concentrations are significant, we mainly consider differences of PM_{2.5} concentration

358 between G4 and RCP4.5/RCP8.5 in our study which we cannot compare these
 359 anomalies with the single RCP4.5 scenario simulated by Li et al. (2023). We do
 360 compare the spatial pattern of differences in PM_{2.5} concentration between “base” and
 361 “EIT1” under RCP4.5. Because of the small slope coefficient of PM_{2.5} emission in our
 362 MLR, we do not capture the large reduction of PM_{2.5} concentration in the Beijing city
 363 center seen by Li et al. (2023), (Fig. S8).
 364

365 **2.7 Relative risks of mortality related to PM_{2.5}**

366 We estimate the effects of PM_{2.5} on mortality by considering changes in the relative risk
 367 (RR) of mortality related to PM_{2.5}. We lack data on mortality rates in the study domain
 368 without which we cannot estimate numbers of fatalities, just the average population-
 369 weighted RR. Burnett et al. (2014) established the integrated exposure-response
 370 functions we use. The RR is non-linear in concentration, that is an initially low PM_{2.5}
 371 region will suffer higher mortality and RR than an initially high PM_{2.5} region if PM_{2.5}
 372 is increased by the same amount. Ran et al. (2023) provide RR values for PM_{2.5}
 373 concentrations up to 200 µg/m³ that includes the 5 main major disease endpoints
 374 (Global Burden of Disease Collaborative Network, 2013) of PM_{2.5} related mortality:
 375 chronic obstructive pulmonary disease, ischemic heart disease, lung cancer, lung
 376 respiratory infection and stroke. We calculate the average population-weighted relative
 377 risks based on the gridded population dataset (Section 2.4) and PM_{2.5} concentration in
 378 the Beijing-Tianjin province defined in the Fig. 1c-1d, following Ran et al. (2023):

$$379 \quad RR_{pop,k} = \frac{\sum_{g=1}^G POP_g \times RR_k(C_g)}{\sum_{g=1}^G POP_g} \quad (5)$$

380 $RR_{pop,k}$ is the average population-weighted relative risk of disease k ($k=1-5$), POP_g is
 381 the population of grid g , and $RR_k(C_g)$ is the relative risk of disease k when PM_{2.5}
 382 concentration is C_g in the grid of g .
 383

384 **2.8 Determination of contributions to change in AP and PM_{2.5}**

385 Equation (1) describes how AP is calculated, and this can be broken down into how
 386 much equivalent temperature is produced by each term (Fig. 3), with 2008-2017 as the
 387 baseline interval for season-by-season contributors to AP. Across scenario seasonal
 388 differences in contributors are then calculated as follows. We use an MLR approach,
 389 since this minimizes the square differences from the mean across the dataset, with the
 390 attendant assumption of independence between the data. Alternatives may also be
 391 considered that e.g. minimize the impact of outliers by considering the magnitude of
 392 the differences, but we prefer to keep the attractive properties of a least squares
 393 approach. The dependent variable in the MLR is the change in AP (ΔAP) and the
 394 independent variables are changes in each factor for each future scenario,

$$395 \quad \Delta AP = \sum \alpha_i X_i + \beta \quad (6)$$

396 where $X_{i(i=1,2,3)}$ are the daily changes of the three meteorological factors between two
 397 scenarios: 2 m temperature (ΔT), 2 m relative humidity (ΔRH) and 10 m wind speed

398 (ΔW), α_i are the regression coefficients of the X_i with ΔAP , and β is the intercept,
 399 which is a constant. We assume that all three meteorological factors should be included
 400 in the regression and we estimate the contributions of each factor to changes of AP as:

$$401 \quad K_i = \frac{\alpha_i \bar{X}_i}{\sum \alpha_i \bar{X}_i} \quad (7)$$

402 where $K_{i(i=1,2,3)}$ is the contributions (in units of temperature) from each factor to the
 403 changes of the AP, and \bar{X}_i are the mean differences in temperature equivalent due to
 404 each factor between two scenarios.

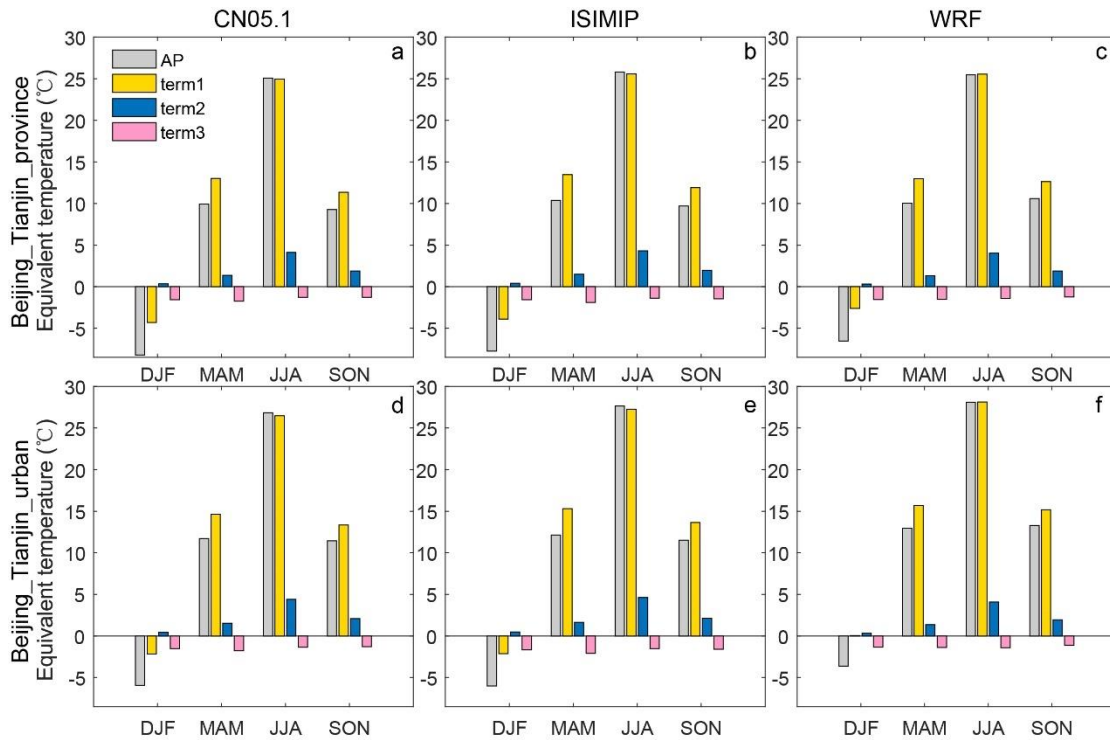
405

406 The contribution of changes in each factor in changes of $PM_{2.5}$ is simpler since we
 407 assume that the relationship between each factor and $PM_{2.5}$ is linear, and so its
 408 contribution is the ratio of product of the regression coefficient and the change of each
 409 factor to the change of $PM_{2.5}$.

410

411 3. Results

412 3.1 Recent apparent temperatures



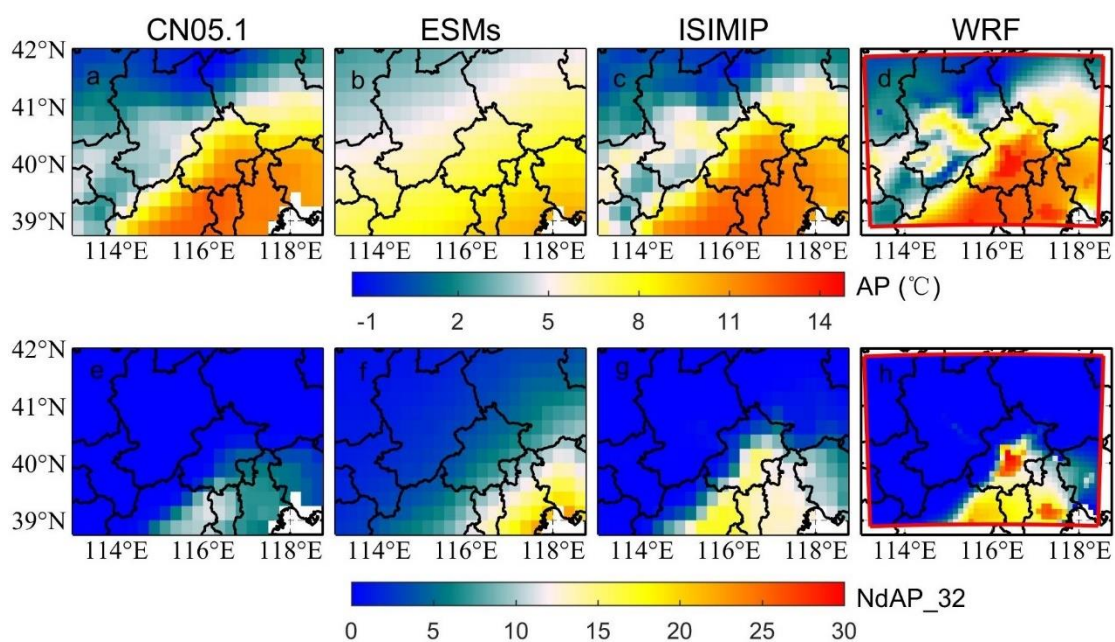
413

414 **Figure 3.** Seasonal averaged AP and equivalent temperature of each term in equation 1 for Beijing-
 415 Tianjin province (a-c) and Beijing-Tianjin urban areas (d-f) during 2008-2017 from CN05.1 (a, d),
 416 4-model ensemble mean after ISIMIP (b, e) and ensemble mean after WRF (c, f). Term 1 is 1.04T, term 2
 417 is 2P and term 3 is -0.65W.

418

419 Figure 3 shows the seasonal averaged AP and equivalent temperatures caused by
 420 temperature, relative humidity and wind speed in Beijing-Tianjin province and Beijing-

421 Tianjin urban areas during 2008-2017. According to the CN05.1 results (Fig. 3a, 3d),
 422 AP and the separate 3 terms show similar seasonal patterns over the whole province
 423 and just the urban areas. Vapor pressure is higher in summer and wind speed is higher
 424 in spring. AP is lower than 2 m temperature in all seasons except summer, and especially
 425 lower in winter. AP, temperature, vapor pressure and wind speed are all higher in urban
 426 areas than in the surrounding rural region in any season. The ISIMIP results (Fig. 3b,
 427 3e), by design, perfectly reproduce the CN05.1 seasonal characteristics of AP,
 428 temperature, vapor pressure and wind speed. WRF shows a similar pattern with that
 429 from CN05.1, but for the Beijing-Tianjin province, WRF overestimates both 2 m
 430 temperature and AP in winter by 2.1°C and by 1.7°C respectively relative to CN05.1
 431 (Fig. 3c). In the Beijing-Tianjin urban areas, WRF overestimates the temperature and
 432 AP relative to CN05.1 in all seasons, especially in winter (Fig. 3f).
 433



434
 435 **Figure 4.** Top row: the spatial distribution of mean apparent temperature from CN05.1 (a), raw ESMS
 436 ensemble mean after bilinear interpolation (b), 4-model ensemble mean after ISIMIP (c) and ensemble
 437 mean after WRF (d) during 2008-2017. Bottom row: the spatial distribution of annual mean number of
 438 days with AP > 32°C from CN05.1 (e), ESMS (f), ISIMIP (e) and WRF (f) during 2008-2017. Fig. S4-S9
 439 and Fig. S5-S10 show the pattern of AP and NdAP_32 for the individual ESM.

440 We compare the simulations of mean apparent temperature and NdAP_32 from both
 441 WRF dynamical downscaling with QDM and from ISIMIP statistical downscaling
 442 during 2008-2017 in Fig. 4. Both WRF with QDM and ISIMIP methods produce a
 443 pattern of apparent temperature which is close to that from CN05.1. While the raw AP
 444 from ESMS is overestimated in Zhangjiakou high mountains and underestimated in the
 445 southern plain, and shares a similar pattern with temperature from ESMS (Wang et al.,
 446 2022). The raw ESM outputs were improved after dynamical and statistical
 447 downscaling. The average annual AP from ISIMIP (9.6-9.7°C) is 0.5°C higher than that
 448 from CN05.1 (9.1°C) over the Beijing-Tianjin province for all ESMS (Table 1). While
 449 WRF produces warmer apparent temperatures in the city centers of Beijing and Tianjin

450 and lower ones in the high Zhangjiakou mountains than recorded in the lower resolution
 451 CN05.1 observations. There are also differences between different models after WRF
 452 downscaling. For example, apparent temperatures from the two MIROC models
 453 downscaled by WRF are the warmest. In contrast AP from all 4 ESMs after ISIMIP
 454 shows very similar patterns (Fig. S4S9).

455
 456 ESMs tend to overestimate the number of days with AP>32°C in southeastern Beijing
 457 and the whole Tianjin province. Both ISIMIP and WRF appear to overestimate the
 458 NdAP_32 in Beijing urban areas and the southerly lowland areas although NdAP_32 is
 459 close to zero in the colder rural areas at relatively high altitude for both downscaling
 460 methods. Some of these differences may be due to the WRF simulations being at finer
 461 resolution than the 0.25°× 0.25° CN05.1, leading to higher probabilities of high AP in
 462 urban areas (Fig. 5d). ISIMIP results also show slight overestimations, especially in the
 463 tails of the distribution (AP>30°C) for urban areas (Fig. 5c). CN05.1 gives about 5
 464 NdAP_32 per year in southern Beijing and Tianjin, but there are nearly 15 NdAP_32
 465 from ISIMIP, and over 20 NdAP_32 per year from WRF downscaling in the Beijing-
 466 Tianjin urban areas during 2008-2017. NdAP_32 from WRF and ISIMIP downscaling
 467 of all ESM is overestimated relative to CN05.1. But there are differences in ESM under
 468 the two downscalings: with ISIMIP, HadGEM2-ES and BNU-ESM have more
 469 NdAP_32 than the two MIROC models, while the reverse occurs with WRF (Fig.
 470 S5S10).

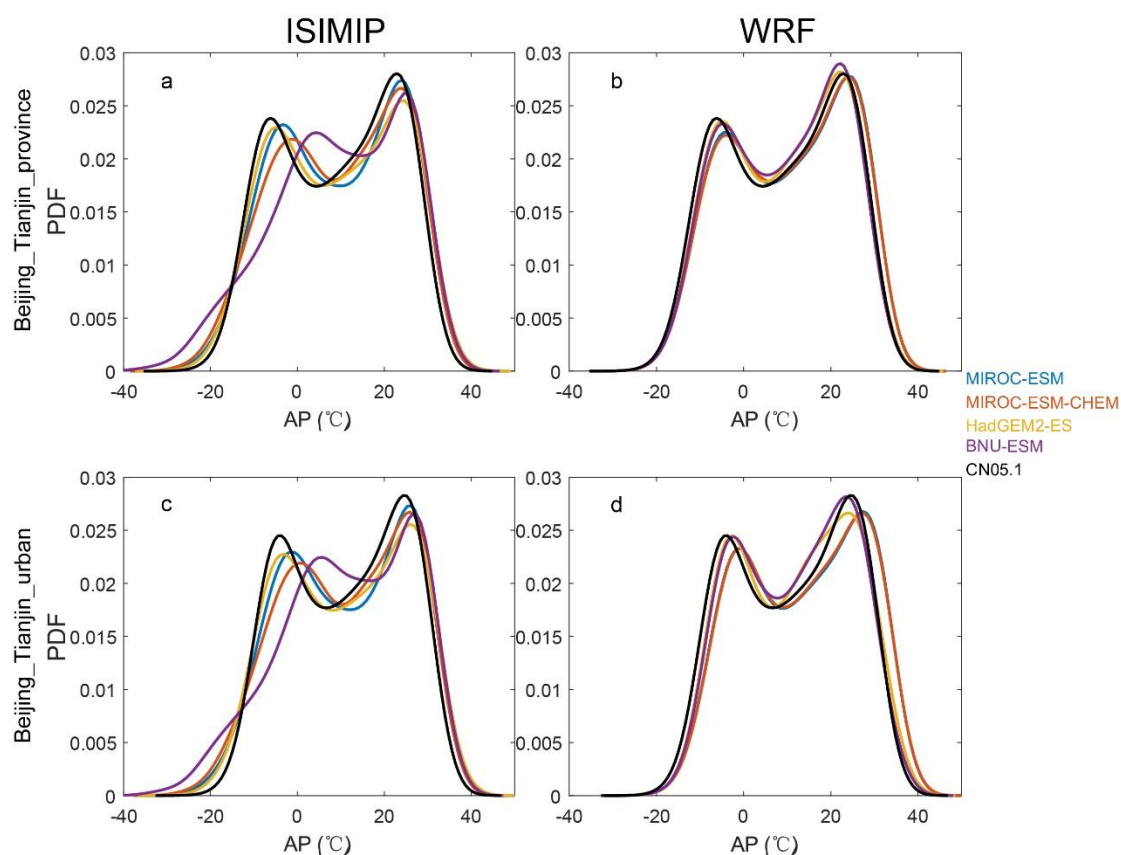
471
 472 **Table 1.** The annual mean apparent temperature and population weighted NdAP_32 in Beijing-Tianjin
 473 province and Beijing-Tianjin urban areas (Fig. 1b) from CN05.1, ISIMIP and WRF during 2008-2017.

Data Sources	AP (°C)				NdAP_32 (day yr ⁻¹)	
	Provinces		Urban		Population weighted for province (Fig. 1c, 1d)	
	WRF	ISIMIP	WRF	ISIMIP	WRF	ISIMIP
MIROC-ESM	10.5	9.6	13.6	11.4	22.2	10.1
MIROC-ESM-CHEM	10.5	9.6	13.6	11.4	21.9	11.0
HadGEM2-ES	9.5	9.6	12.0	11.4	12.3	11.1
BNU-ESM	9.4	9.7	11.8	11.5	10.2	12.7
CN05.1	9.1		11.1		2.4	

474 The Taylor diagram of the daily mean apparent temperature in Beijing-Tianjin province
 475 and Beijing-Tianjin urban areas from 2008-2017 for the 4 ESMs shows that correlation
 476 coefficients between ESMs and CN05.1 are greater than 0.85 under both downscaling
 477 methods. Although there are differences between ESMs, the performance of WRF, with
 478 higher correlation coefficient and smaller SD (standard deviation) and RMSD (root
 479 mean standard deviation), is usually superior to ISIMIP (Fig. S6S11). Taking the
 480 Beijing-Tianjin urban areas as an example (Fig. S611bb), under the ISIMIP method,
 481 MIROC-ESM, MIROC-ESM-CHEM and HadGEM2-ES have the same correlation
 482 coefficient (0.92) and RMSD (5.4°C) with the CN05.1, while BNU-ESM has lower
 483 correlation coefficient (0.88) and higher RMSD (7.0°C). Under WRF simulations,

484 MIROC-ESM and MIROC-ESM-CHEM have larger correlation coefficients and
 485 smaller RMSD with CN05.1 than HadGEM2-ES and BNU-ESM.

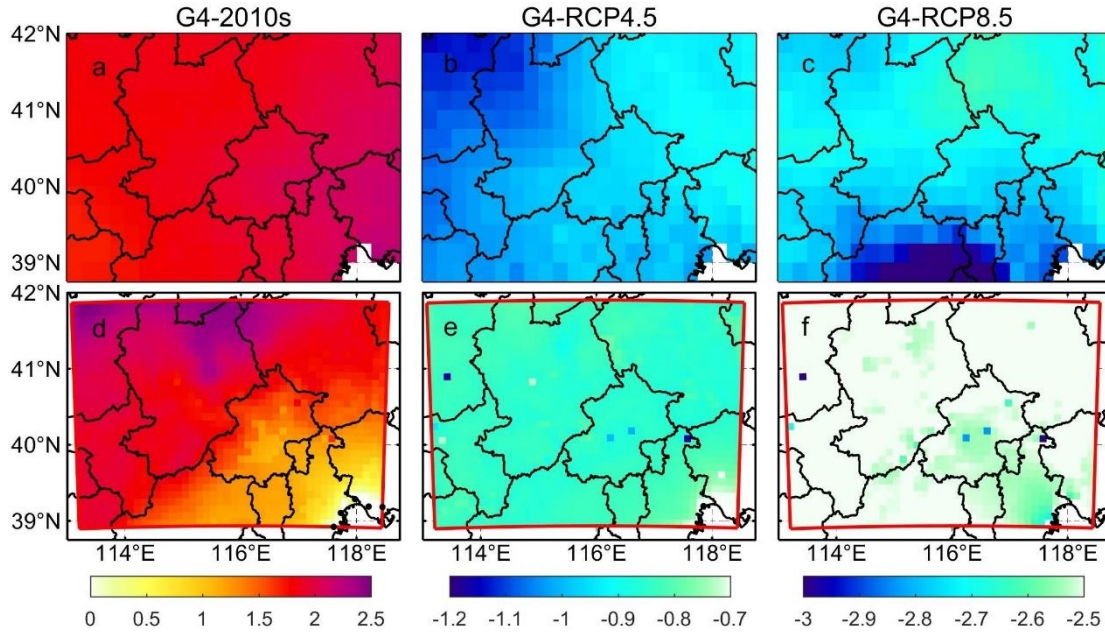
486 Figure 5 shows the probability density functions (pdf) of daily AP from the four ESMS
 487 under ISIMIP and WRF in Beijing-Tianjin province and Beijing-Tianjin urban areas
 488 during 2008-2017. ISIMIP overestimates the probability of extreme cold AP relative to
 489 CN05.1 (especially BNU-ESM), although all ESM reproduce the CN05.1 pdf well at
 490 high AP. WRF can reproduce the CN05.1 distribution of AP better than ISIMIP, but
 491 high AP is overestimated relative to CN05.1 and the urban areas perform less well than
 492 the whole Beijing-Tianjin province. In urban areas all ESMs driving WRF tend to
 493 underestimate the probability of lower AP and to overestimate the probability of higher
 494 AP, especially the two MIROC models (Fig. 5d). Fig. [S7-S12](#) displays the annual cycle
 495 of monthly AP, with ISIMIP proving excellent by design, at reproducing the monthly
 496 AP. While under WRF downscaling AP shows more across model differences,
 497 especially during summer and with greater spread for the urban areas.



498
 499 **Figure 5.** The probability density function (pdf) for daily apparent temperature under ISIMIP (a, c) and
 500 WRF (b, d) results in Beijing-Tianjin province (a, b) and Beijing-Tianjin urban areas (c, d) during 2008-
 501 2017.

502 3.2 2060s apparent temperatures

503 3.2.1 Changes of apparent temperature



504

505 **Figure 6.** Spatial pattern of ensemble mean apparent temperature difference (°C) under different
 506 scenarios over 2060-2069: G4-2010s (left column), G4-RCP4.5 (middle column) and G4-RCP8.5 (right
 507 column) based on ISIMIP and WRF methods. 2010s refers to the 2008-2017 period. Stippling indicates
 508 grid points where differences or changes are not significant at the 5% level according to the Wilcoxon
 509 signed rank test.

510

511 Figure 6 shows the ISIMIP and WRF ensemble mean changes in the annual mean AP
 512 under G4 during 2060-2069 relative to the past and the two future RCP scenarios.
 513 ISIMIP-downscaled AP (Fig. 6a-6c) shows significant anomalies ($p < 0.05$), with whole
 514 domain rises of 2.0 °C in G4-2010s, and falls of 1.0 °C and 2.8 °C in G4-RCP4.5 and
 515 G4-RCP8.5 respectively. In WRF results, AP under G4 is about 1-2 °C warmer than
 516 that under 2010s, 0.8 °C and 2.5 °C colder than that under RCP4.5 and RCP8.5 over
 517 the whole domain. Individual ESM results downscaled by ISIMIP and WRF are in Fig.
 518 [S9-S14](#) and Fig. [S10-S15](#). For both ISIMIP and WRF downscaling results, the two
 519 MIROC models show stronger warming than the other two models between G4 and the
 520 2010s. WRF-downscaled AP driven by HadGEM2-ES exhibits the strongest cooling,
 521 with decreases of 1.7 °C between G4 and RCP4.5 and falls of 3.0 °C between G4 and
 522 RCP8.5. Although different ESMs show different changes in AP between G4 and other
 523 scenarios, changes in AP are almost the same everywhere for a given ESM in the
 524 ISIMIP results (Fig. [S9-S14](#)). WRF-downscaled AP anomalies driven by two MIROC
 525 models are larger in the Zhangjiakou mountains and smaller in the Beijing urban areas
 526 and Tianjin city between G4 and 2010s (Fig. [S10-S15](#)). Changes in AP from ISIMIP
 527 results, whether across whole province or just the urban areas, are statistically identical
 528 given scenarios (Table 2), which is consistent with patterns in figure 6. AP under G4 is
 529 0.8 °C (1.0 °C) and 2.6 °C (2.8 °C) colder than that under RCP4.5 and RCP8.5 in
 530 Beijing-Tianjin urban areas from ISIMIP (WRF) results. The warming between G4 and
 531 2010s in urban areas is 1.0 °C in WRF results, while that is 2.0 °C in ISIMIP results
 532 (Table 2).

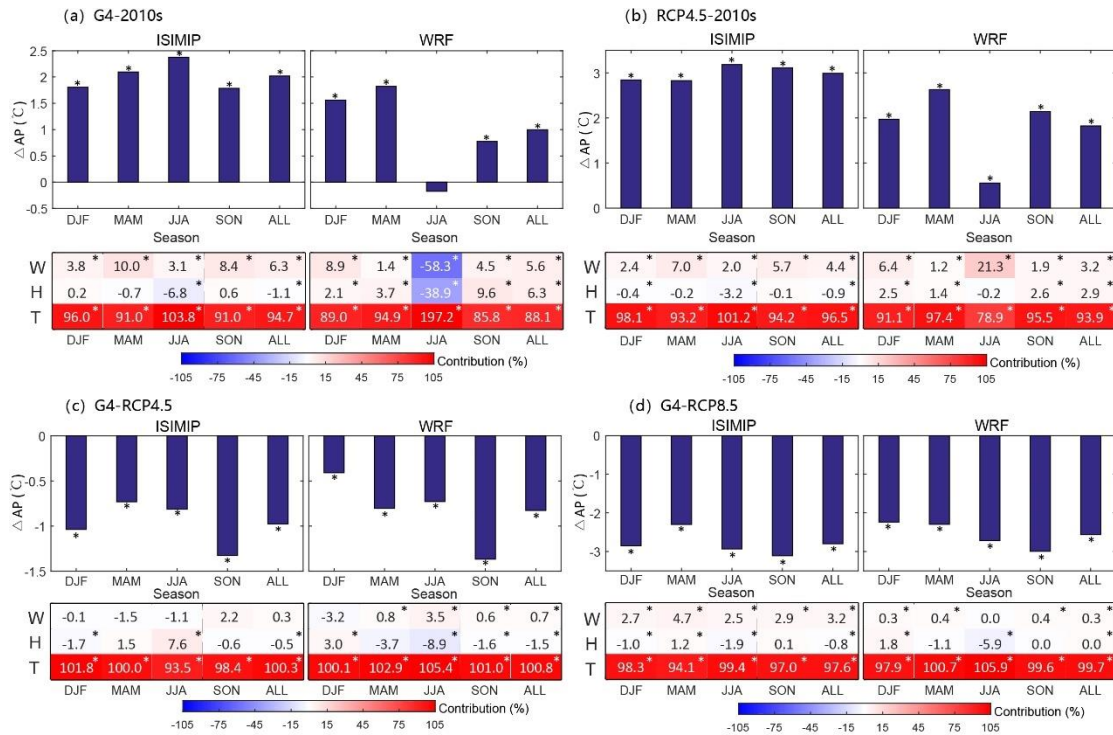
533

534 **Table 2.** Difference of apparent temperature between the G4 and other scenarios for the Beijing-Tianjin
 535 province and Beijing-Tianjin urban areas as defined in Fig. 1b during 2060-2069. Bold indicates the
 536 differences or changes are significant at the 5% level according to the Wilcoxon signed rank test.
 537 (Units: °C)

Model	G4-2010s				G4-RCP4.5				G4-RCP8.5			
	WRF		ISIMIP		WRF		ISIMIP		WRF		ISIMIP	
	Urban	Province	Urban	Province	Urban	Province	Urban	Province	Urban	Province	Urban	Province
MIROC-ESM	0.9	1.5	2.2	2.2	-0.5	-0.4	-0.9	-0.9	-2.3	-2.1	-2.8	-2.7
MIROC-ESM-CHEM	0.9	1.5	2.9	2.8	-0.4	-0.4	-0.1	-0.1	-2.0	-2.0	-2.1	-2.1
HadGEM2-ES	1.1	1.0	1.8	1.7	-1.6	-1.6	-1.6	-1.6	-3.1	-3.1	-3.3	-3.3
BNU-ESM	1.2	1.1	1.2	1.3	-0.8	-0.8	-1.3	-1.3	-2.8	-2.7	-2.9	-2.9
Ensemble	1.0	1.3	2.0	2.0	-0.8	-0.8	-1.0	-1.0	-2.6	-2.5	-2.8	-2.8

538

539 **3.2.2 Contributing factors to changes in AP**



540

541 **Figure 7.** The seasonal changes of AP (ΔAP) and the seasonal contribution of climatic factors to ΔAP
 542 for Beijing and Tianjin urban areas under ISIMIP and WRF between G4 and 2010s **(a)**, G4 and 2010s
 543 **(b)**, G4 and RCP4.5 **(c)** and G4 and RCP8.5 **(d)** in the 2060s based on ensemble mean results. Colors
 544 and numbers in each cell correspond to color bar, and “*” above the columns and in the cells indicate
 545 differences are significant at the 5% significant level under the Wilcoxon test.

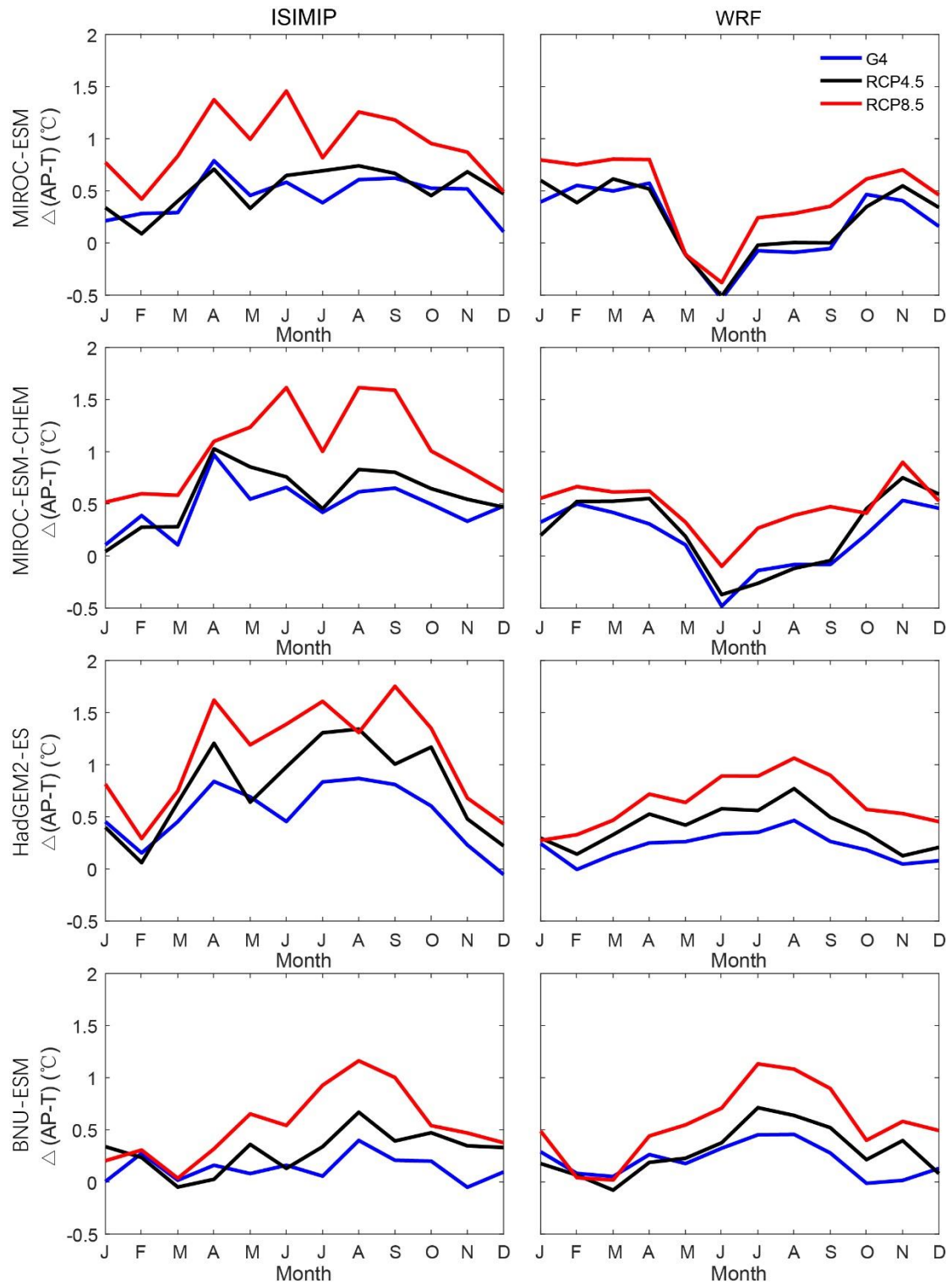
546

547 Figure 7 shows the ISIMIP and WRF ensemble mean changes in the annual mean AP
 548 anomalies G4 during 2060-2069 relative to the past and the two future RCP scenarios.
 549 ISIMIP-downscaled AP (Fig. 7a-7c) shows significant anomalies ($p < 0.05$) across the
 550 whole domain, even for the relatively small differences in G4-RCP4.5. ΔAP by WRF

551 is lower than that by ISIMIP. Between G4 and 2010s, AP are projected to have increases
552 of 1.8 (1.6), 2.1 (1.8), 2.4 (-0.2), 1.8 (0.8) °C from winter to autumn in ISIMIP (WRF)
553 results. In ISIMIP results, the contribution of temperature ranges from 91%-104%, and
554 the contribution of wind speed ranges from 3%-10% in all seasons, while the
555 contribution of humidity is negative or insignificant (Fig. 7a). However, the
556 contribution of humidity is positive in WRF results (Fig. 7a). Between RCP4.5 and
557 2010s, annual mean AP is projected to increase by 3.0 °C and 1.8 °C in ISIMIP and
558 WRF results respectively, which is higher than that between G4 and 2010s. The increase
559 of temperature and decrease of wind speed have a significant impact on the annual
560 average Δ AP contributed 97% (94%) and 4% (3%) in ISIMIP (WRF) results. The
561 contributions of changes in humidity are significantly positive under G4 and RCP4.5 in
562 WRF results, while it is the opposite in the ISIMIP results (Fig. 7a-7b).

563

564 Relative to RCP4.5 in the 2060s, AP is projected to decrease by 1.0 (0.4), 0.7 (0.8), 0.8
565 (0.7), and 1.3 (1.4) °C from winter to autumn under G4 in ISIMIP (WRF) results (Fig.
566 7c). In summer, the contribution from changes in temperature and humidity are 94%
567 (105%) and 8% (-9%) in ISIMIP (WRF) results, respectively. There are insignificant
568 contributions from wind speed under ISIMIP results, but a significant slight positive
569 contribution (0.7%-4%) under WRF results (Fig. 7c). The annual mean AP under G4 is
570 2.8 (2.6) °C lower than that under RCP8.5 in ISIMIP (WRF) result. In this case, the
571 contribution of changes in wind on Δ AP ranges from 3%-5% by ISIMIP, while it is
572 close to 0 by WRF. As expected, Δ AP is mainly determined by the changes in
573 temperature, with contributions usually above 90% between different scenarios.



574

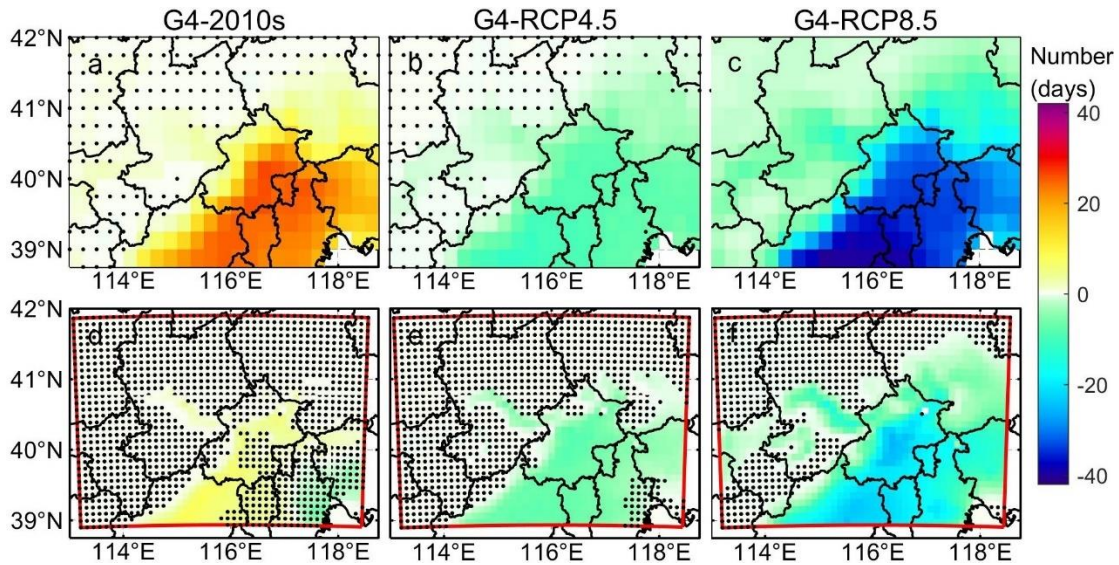
575 **Figure 8.** The change of apparent temperature based on air temperature under three scenarios (G4,
 576 RCP4.5 and RCP8.5) in four ESMs under ISIMIP (left column) and WRF (right column) for urban areas
 577 relative to the 2010s.

578

579 A useful measure of heat impacts that may be missed if considering only at air
 580 temperatures is the seasonality of the differences between AP and air temperature
 581 ($\Delta(AP-T)$; Fig. 8). The four model ensemble annual mean $\Delta(AP-T)$ under ISIMIP is

582 projected to rise by 0.4°C, 0.5°C and 0.9°C under G4, RCP4.5 and RCP8.5, relative to
 583 the 2010s. Under WRF, $\Delta(\text{AP-T})$ is much smaller than under ISIMIP but still rising
 584 faster than air temperatures: by 0.2°C, 0.3°C and 0.5°C under G4, RCP4.5 and RCP8.5
 585 relative to the 2010s, respectively. In general, the largest anomalies in $\Delta(\text{AP-T})$ are in
 586 summer under both WRF and ISMIP downscaling, but the two MIROC models under
 587 WRF have small or even negative $\Delta(\text{AP-T})$ in summer with WRF.

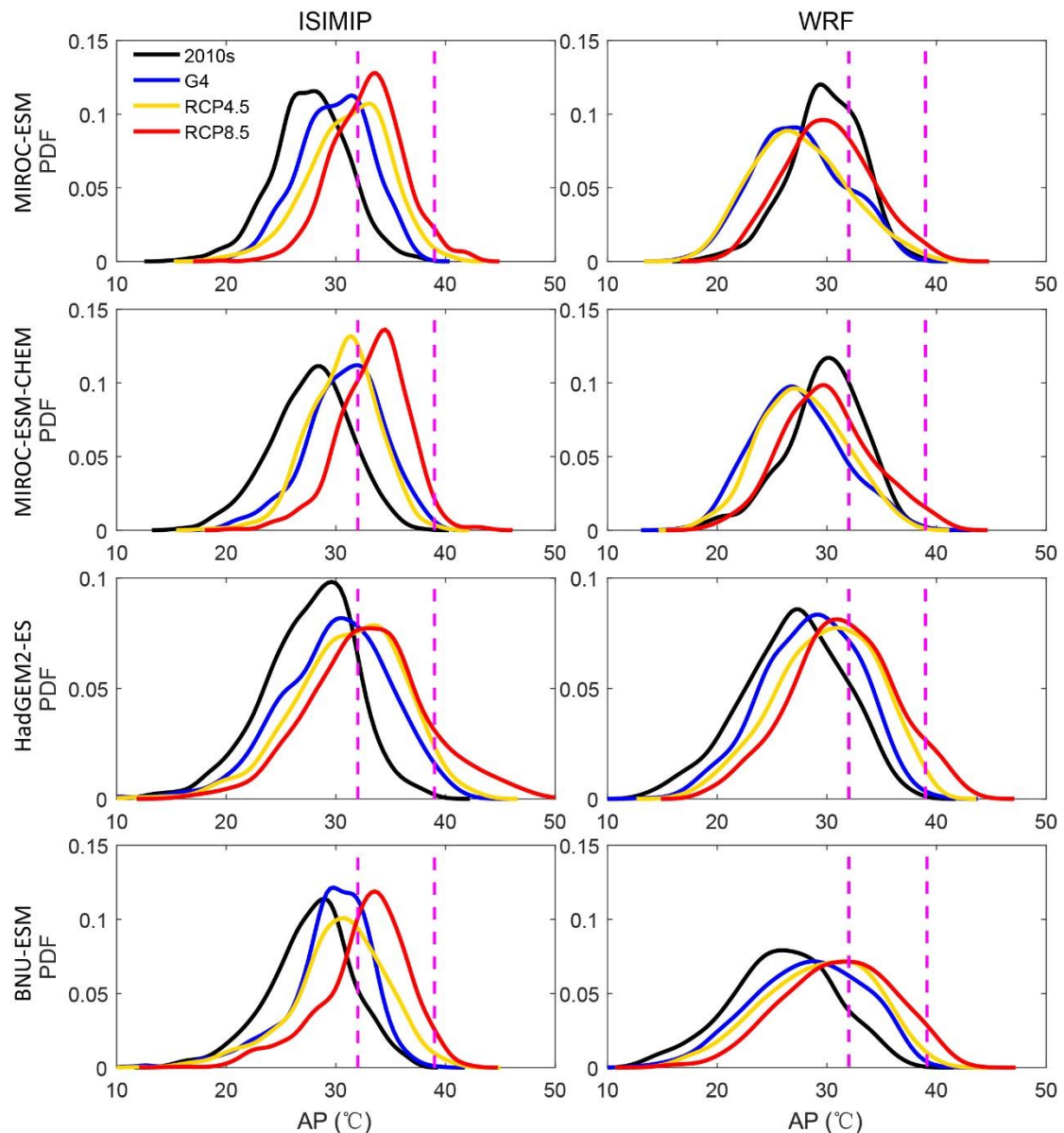
588 3.2.3 Changes of the number of days with $\text{AP} > 32^\circ\text{C}$



589 **Figure 9.** Ensemble mean differences in annual number of days with $\text{AP} > 32^\circ\text{C}$ (NdAP_{32}) between
 590 scenarios for 2060-2069: G4-2010s (left column), G4-RCP4.5 (second column) and G4-RCP8.5 (right
 591 column) based on ISIMIP method and WRF. 2010s means the results simulated during 2008-2017.
 592 Stippling indicates grid points where differences or changes are not significant at the 5% level according
 593 to the Wilcoxon signed rank test. Corresponding ISIMIP results for each ESM are in Fig. [S11S16](#), and
 594 WRF results in Fig. [S12S17](#).
 595

596
 597 The NdAP_{32} anomalies in Figure 9 show that ISIMIP projects an increase of about 20
 598 days per year with $\text{AP} > 32^\circ\text{C}$ for the southeast of Beijing province and 10 days in the
 599 western areas of Beijing under G4 relative to the 2010s. NdAP_{32} is about 10 days
 600 fewer under G4 than RCP4.5 with no clear spatial differences. G4 has about 35 fewer
 601 NdAP_{32} days in the southern part of the domain and 20 fewer days in the western
 602 domain than the RCP8.5 scenario. In contrast WRF suggests that most areas do not
 603 show any significant difference between G4 and the 2010s, while the anomalies relative
 604 to RCP4.5 are similar as ISIMIP, the differences are insignificant over more area than
 605 ISIMIP. G4-RCP8.5 anomalies with WRF are smaller than with ISIMIP, and differences
 606 are not significant in the Zhangjiakou high mountains. The urban areas show larger
 607 decreases in NdAP_{32} than the more rural areas, even in the low altitude plain.
 608 Individual ESM show almost no statistically significant differences between G4 and
 609 RCP4.5 (Fig. [S11-S16](#) and [S12S17](#)), but the differences seen in Fig. 9 are significant
 610 because of the larger sample size in the significance test. All ESMs with ISIMIP show
 611 more NdAP_{32} in the urban areas under G4 than the 2010s, while two MIROC models

612 driving WRF show fewer NdAP_32 in Beijing-Tianjin urban areas (Fig. S11S16,
 613 S12S17).
 614



615
 616 **Figure 10.** Probability density distributions of daily apparent temperature (AP) in summer (JJA) over
 617 Beijing-Tianjin urban areas under recent period (2008-2017), and the 2060s under G4, RCP4.5 and
 618 RCP8.5 scenarios from ISIMIP and WRF results. The purple dotted lines are at AP of 32°C and 39°C.

619
 620 The pdf of daily apparent temperature in summer over Beijing-Tianjin urban areas (Fig.
 621 10) shifts rightwards for G4, RCP4.5 and RCP8.5 during the 2060s relative to the 2010s.
 622 Figure 10 shows that by the 2060s, the dangerous threshold of AP>39 is crossed
 623 frequently under RCP8.5 with both WRF and ISIMIP downscaling, but for the RCP4.5
 624 and G4 scenarios these events are much rarer. ISIMIP results tend to show higher
 625 probability tails (extreme events) than under WRF simulations.

626

627 Population weighted NdAP_32 in the 2060s for Beijing-Tianjin province is shown in
 628 Table 3. ISIMIP downscaling suggests ensemble mean rises in NdAP_32 of 22.4 days
 629 per year under G4 relative to the 2010s, but that G4 has 8.6 and 33.5 days per year
 630 fewer than RCP4.5 and RCP8.5, respectively. NdAP_32 from WRF under G4 is
 631 reduced by 19.6 days per year relative to RCP8.5, and by 6.3 days relative to RCP4.5
 632 (Table 3).

633

634 **Table 3.** Difference of population weighted NdAP_32 between the G4 and other scenarios for Beijing-
 635 Tianjin province (Fig. 1c, 1d) during 2060-2069. Bold indicates the changes are significant at the 5%
 636 level according to the Wilcoxon signed rank test. (Units: day y⁻¹).

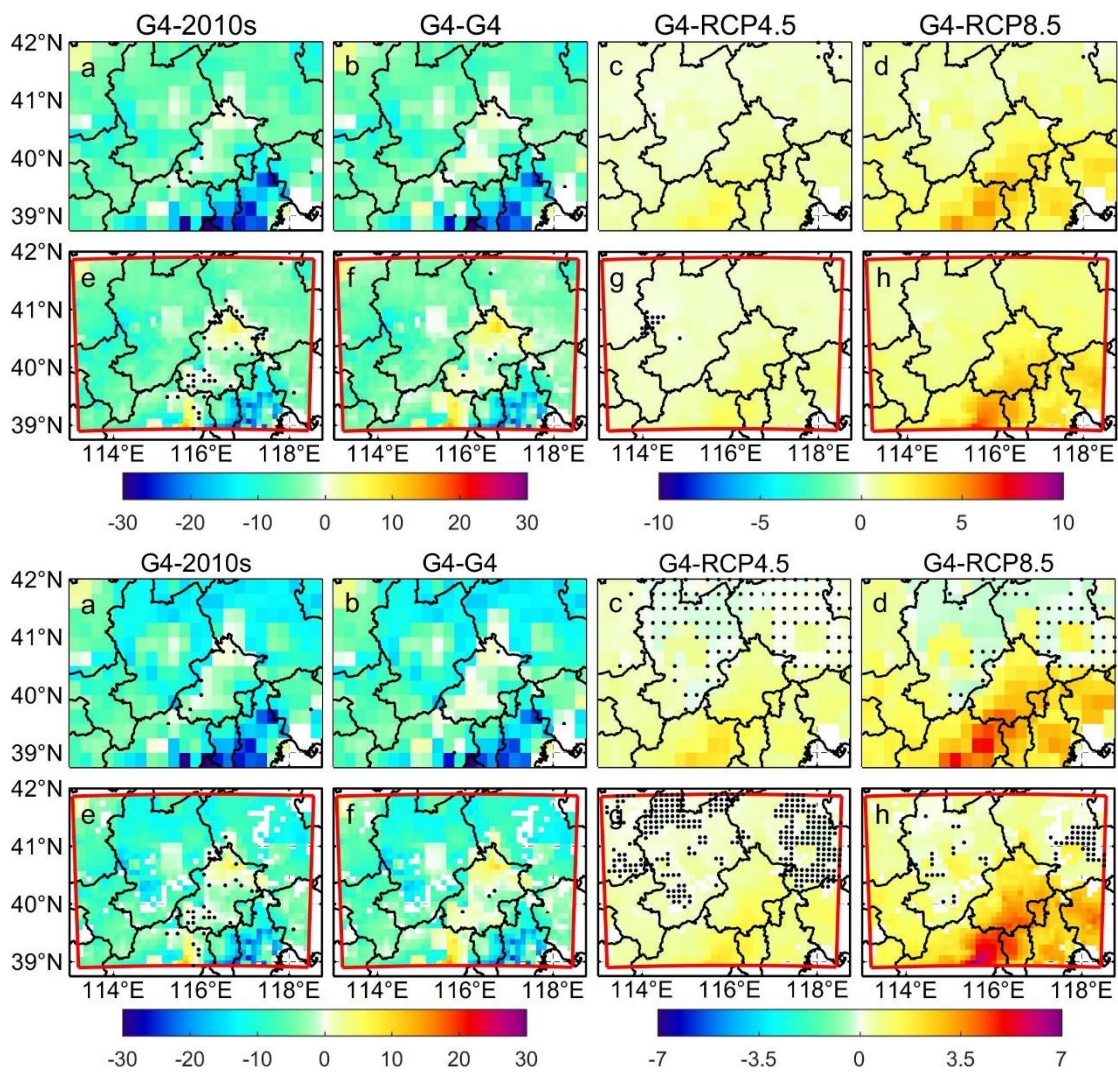
637

Beijing-Tianjin province	G4-2010s		G4-RCP4.5		G4-RCP8.5	
	ISIMIP	WRF	ISIMIP	WRF	ISIMIP	WRF
MIROC-ESM	18.6	-8.1	-17.0	0.8	-35.4	-13.1
MIROC-ESM-CHEM	28.7	-10.2	3.9	-2.2	-33.7	-15.5
HadGEM2-ES	25.7	9.4	-12.5	-13.5	-24.3	-25.3
BNU-ESM	16.4	13.6	-8.6	-10.4	-40.5	-24.4
Ensemble	22.4±2.9	1.2±6.0	-8.6±4.5	-6.3±3.4	-33.5±3.4	-19.6±3.1

638

639 **3.3 PM_{2.5} in the 2060s**

640 **3.3.1 PM_{2.5} scenarios in the 2060s**



641

642

643 **Figure 11.** Spatial patterns of ensemble mean PM_{2.5} concentration difference (µg/m³) between
 644 “mitigation” under G4 in the 2060s and reference (a, e), between “mitigation” and “baseline” under
 645 G4 in the 2060s (b, f), between G4 and RCP4.5 under “mitigation” scenario in the 2060s (c, g), and
 646 between G4 and RCP8.5 under “mitigation” scenario in the 2060s (d, h) based on ISIMIP (a-d) and
 647 WRF (e-h) results. Excessive collinearity variables have been removed (Fig. S18 shows the results
 648 without this procedure). –Stippling indicates grid points where differences or changes are not
 649 significant at the 5% significant level according to the Wilcoxon signed rank test.

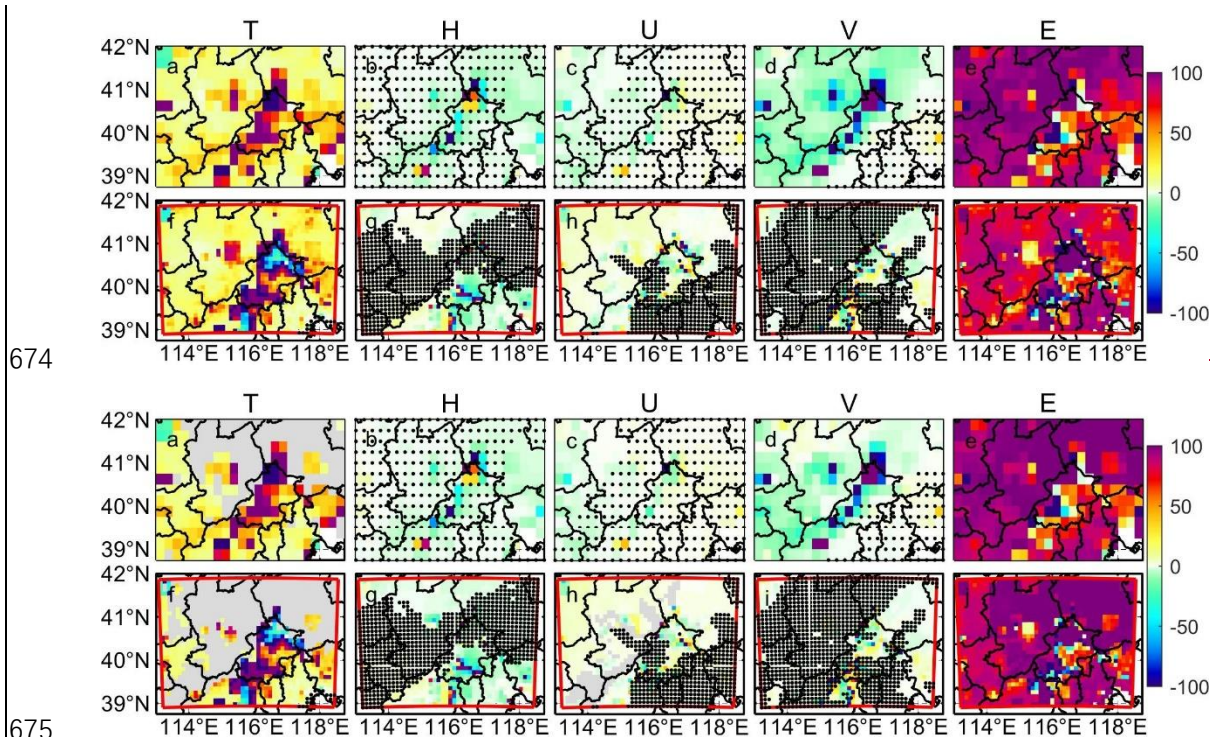
650

651 We firstly project the change of PM_{2.5} under G4 and the aerosol mitigation scenario in
 652 2060s relative to 2010s (Fig. 11a, e). Both ISIMIP and WRF project PM_{2.5} decreases in
 653 most areas, especially in Tianjin and Langfang, but PM_{2.5} decreases more under ISIMIP
 654 than WRF. PM_{2.5} concentration decreases by ~~6.57.6~~ 6.57.6 µg/m³ over Beijing-Tianjin
 655 province in ISIMIP, and decrease by ~~4.35.4~~ 4.35.4 µg/m³ in WRF (Table S2S3). PM_{2.5}
 656 concentration is 0.5-8 µg/m³ higher in northern Beijing under G4 (“mitigation”) than
 657 that during the 2010s in WRF. To show the impact of emission reductions, we compare
 658 the PM_{2.5} concentration between aerosol “baseline” and “mitigation” scenarios under
 659 G4 in the 2060s (Fig. 11b, 11f), and compare the “mitigation” PM_{2.5} concentration

660 under G4 and the RCP scenarios in the 2060s to clarify the effect of geoengineering
 661 compared with climate warming. Compared with “baseline” scenario, PM_{2.5}
 662 concentration is less under “mitigation” scenario as expected in both ISIMIP and WRF
 663 under G4 (Fig. 11b, 11f), and has a similar spatial pattern with that in Fig. 11a and 11e.
 664 Compared with RCP4.5 and RCP8.5, PM_{2.5} concentration under G4 are higher over the
 665 Beijing-Tianjin province in ISIMIP results (Fig. 11c-11d), but with large differences
 666 between the 4 ESMs. G4 PM_{2.5} is simulated greater than in RCP scenarios under
 667 HadGEM2-ES and BNU-ESM (Fig. S13kS19k, l, o, p), but there are insignificant
 668 differences in most areas under the two MIROC models (Fig. S13eS19c, d, g, h). PM_{2.5}
 669 concentrations are larger between G4 and RCP8.5. WRF simulations shows similar
 670 changes in PM_{2.5} between G4 and RCPs as ISIMIP over Beijing-Tianjin province (Fig.
 671 11g-h).

672

673 3.3.2 PM_{2.5} meteorological and emissions controls in the 2060s

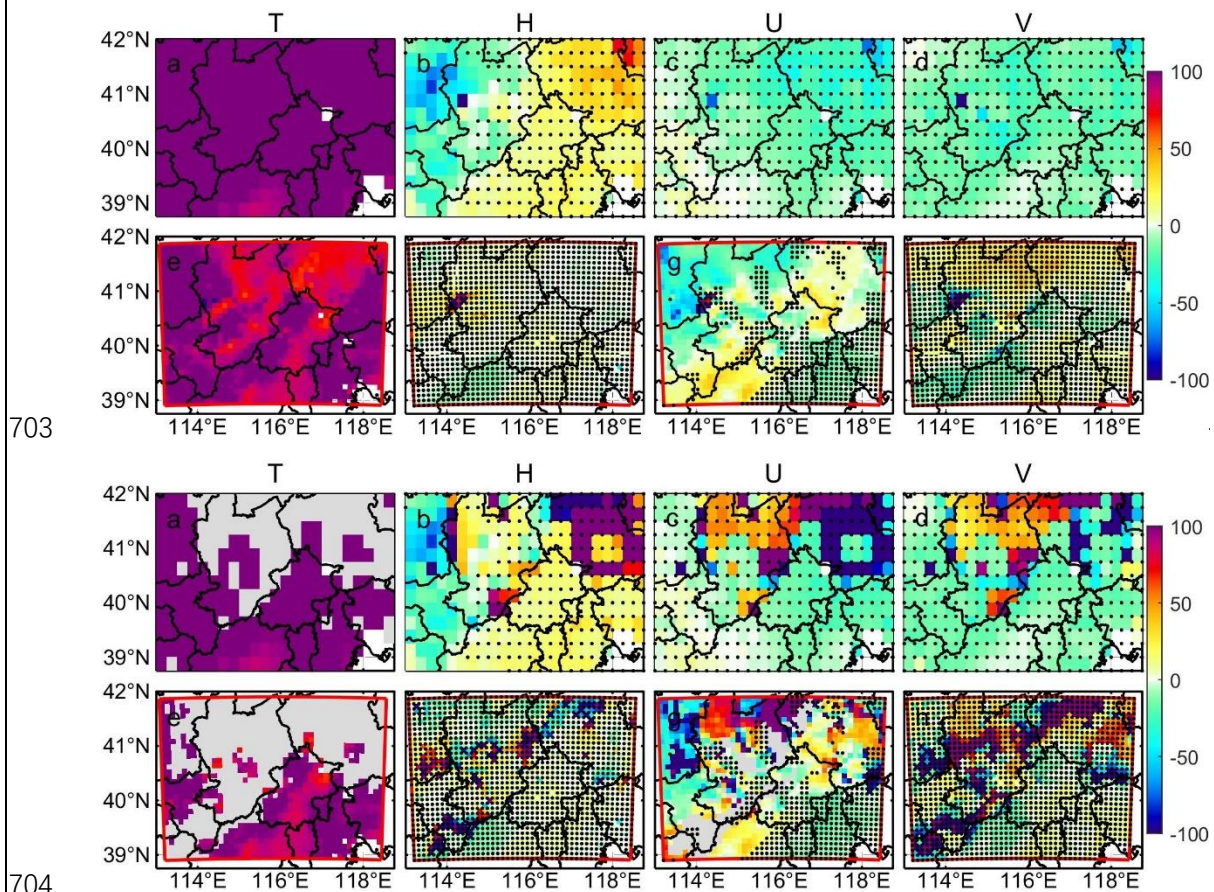


676 **Figure 12.** Contribution of climate factors (temperature/T, humidity/H, zonal wind/U, meridional
 677 wind/V) and emission (E) to changes in monthly PM_{2.5} concentration (Δ PM_{2.5}) in 2060s under G4
 678 (“mitigation”) relative to 2010s. Top figures (a-e) are ISIMIP results, and bottom figures (f-j) are
 679 WRF results. Stippling indicates the changes are insignificant at the 5% significant level in the
 680 Wilcoxon test. The grey areas represent the collinearity in the MLR, and they exist in the panel a, f
 681 and h.

682

683 Next, we quantify the contribution of different meteorological factors and PM_{2.5}
 684 emissions to Δ PM_{2.5} between G4 (“mitigation”) in the 2060s and the 2010s (Fig. 12).

685 Both ISIMIP and WRF results show that the increase of temperature and decrease of
 686 PM_{2.5} emission play positive roles in reducing PM_{2.5} concentration. ISIMIP results (Fig.
 687 12a-e), suggest that the projected increase of temperature could explain 0-20% of the
 688 decrease of PM_{2.5} concentration, and decrease of PM_{2.5} emission could explain more
 689 than 90% of changes in PM_{2.5} concentration differences in most of areas. Changes in
 690 humidity and westerly winds (positive U-wind) do not cause significant changes in
 691 ΔPM_{2.5}, but projected increases southerly wind (positive V-wind) is detrimental to the
 692 decrease in PM_{2.5} concentration, and has a 0-10% negative effect on ΔPM_{2.5} in
 693 Zhangjiakou. WRF results show similar spatial pattern in effect of temperature and
 694 emission on ΔPM_{2.5} with ISIMIP results. Although temperature is projected to increase
 695 over the whole domain (Fig. S16S22), there are negative contributions on ΔPM_{2.5} to the
 696 north of Beijing due to increase of PM_{2.5} caused by the negative correlation between
 697 PM_{2.5} and its emissions (Fig. S20S26). The ~1-2% ~~wetter-increase of humidity~~ ~~has leads~~
 698 ~~to ~10% ~10% negative effect on decrease~~ ~~increase~~ of PM_{2.5} ~~concentration in the~~ south
 699 of Beijing (Fig. 12g), and 0.2-0.3 m/s decreases of U-wind ~~have leads to~~ 0-10% ~~negative~~
 700 ~~contribution on decrease~~ ~~increase~~ of PM_{2.5} ~~concentration~~ in Zhangjiakou (Fig. 12h). The
 701 changes in each factor in ISIMIP and WRF results are shown in Fig. S15-S21 and Fig.
 702 S16S22, respectively.



705 **Figure 13.** Contribution of climate factors (as in Fig. 12) to changes in monthly PM_{2.5} concentration
 706 in 2060s under G4 with aerosol “mitigation” relative to 2060s under RCP4.5 with aerosol
 707 “mitigation”. Top figures (a-e) are ISIMIP results, and bottom figures (f-j) are WRF results.
 708 Stippling indicates the changes are insignificant at the 5% significant level in the Wilcoxon test. The

709 grey areas represent the collinearity in the MLR, and they exist in the panel a, f and h.

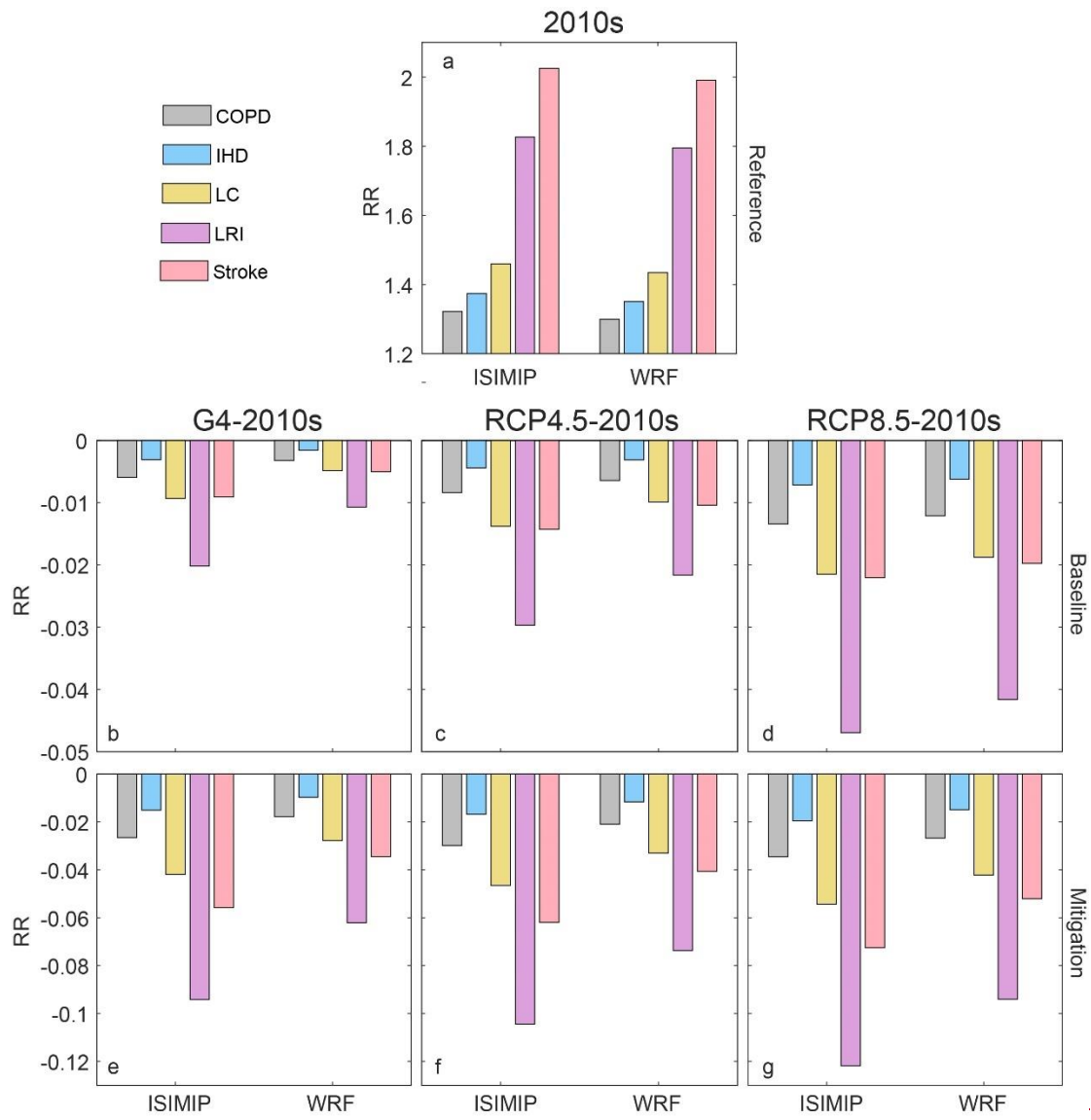
710

711 Now we explore the contribution of each meteorological factor to $\Delta PM_{2.5}$ between G4
712 (“mitigation”) and RCP4.5 (“mitigation”) in the 2060s (Fig. 13). The higher $PM_{2.5}$
713 under G4 is mainly caused by the lower temperature. In ISIMIP, lower temperature
714 explains more than 90% (100% in some places) of the raised $PM_{2.5}$ relative to RCP4.5,
715 although the increase of humidity is also helpful to lower $PM_{2.5}$ in the western domain
716 (Fig. 13a-b). Humidity can increase suspended particle mass and coagulation,
717 promoting deposition (Li et al., 2015). The contribution of differences in U-wind and
718 V-wind on $\Delta PM_{2.5}$ is insignificant (Fig. 13c-d). In WRF, the projected lower
719 temperatures explain more than 70% of the higher $PM_{2.5}$ under G4 relative to RCP4.5
720 (Fig. 13e). Although the increase of southerly (V) wind contributes 10-20% to the
721 higher $PM_{2.5}$ in the northern domain under HadGEM2-ES and BNU-ESM (Fig.
722 S18S24), it is insignificant in the ensemble (Fig. 13h). Decreased westerlies (U wind)
723 explains about between +20100% and -20100% of $PM_{2.5}$ differences (Fig. 13g), since
724 U-wind impacts vary spatially (Fig. S20S26).

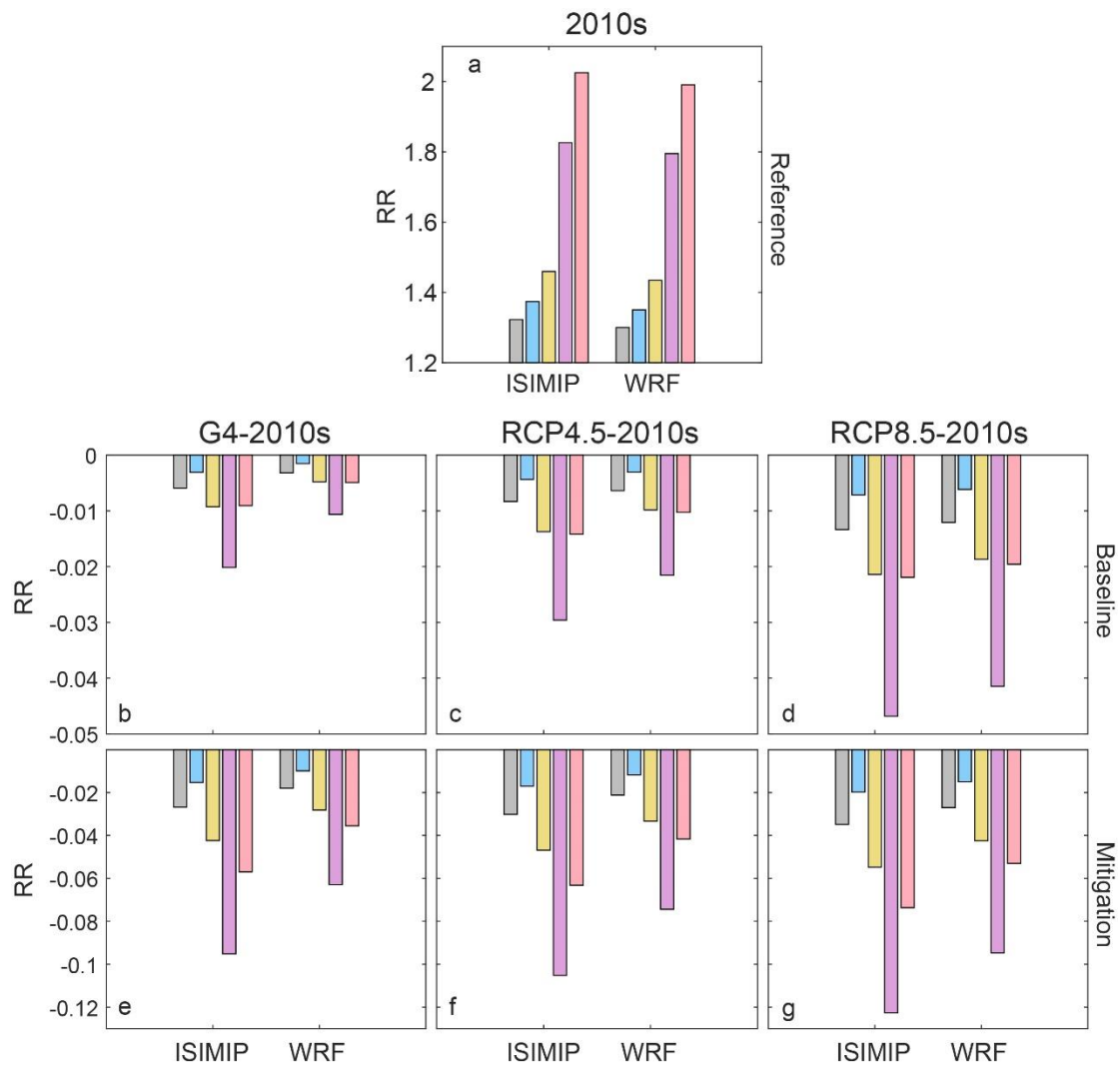
725

726 **3.3.3 $PM_{2.5}$ impact on health risks now and in the 2060s**

727 Changes in RR of $PM_{2.5}$ for the 5 diseases under the geoengineering and global
728 warming climate scenarios and different emission scenarios during 2060s relative to
729 2010s for the Beijing-Tianjin province are shown in Fig. 14. Present-day $PM_{2.5}$ related
730 RRs are 1.32 (1.30), 1.37 (1.35), 1.46 (1.43), 1.83 (1.80) and 2.02-03 (1.99) for chronic
731 obstructive pulmonary disease (COPD), ischemic heart disease (IHD), lung cancer (LC),
732 lung respiratory infection (LRI) and stroke according to the ISIMIP (WRF) simulations
733 (Fig. 14a). RR of LRI is the highest and COPD is the lowest in the five diseases, and
734 WRF estimates of RR are 0.02-0.03 lower than those of ISIMIP. In both the “baseline”
735 and “mitigation” emission scenarios, RRs will be lower under G4, RCP4.5 and RCP8.5
736 compared with the 2010s. Smaller RR reductions occur under G4 than under RCP4.5
737 and RCP8.5, and ISIMIP simulates larger reductions than WRF. This is because the
738 $PM_{2.5}$ concentrations from ISIMIP are reduced more than with WRF (Table S2S3).
739 Under the “baseline” emission scenario (Fig. 14b-d), the biggest reduction of RR for
740 LRI is 0.047 under RCP8.5 in ISIMIP, and RRs for other diseases are projected to
741 reduce by no more than 0.02. Under the “mitigation” emission scenario (Fig. 14e-g),
742 reductions in RRs are 3-6 times greater.



743



744

745 **Figure 14.** Average population-weighted relative risks of PM_{2.5} related 5 diseases in 2010s (a) and
 746 its changes between G4 and 2010s (b, e), between RCP4.5 and 2010s (c, f) and between RCP8.5
 747 and 2010s (d, g) in Beijing-Tianjin province based on the ISIMIP and WRF results, respectively.
 748 PM_{2.5} concentration is based on the “baseline” emissions under G4, RCP4,5 and RCP8.5 in the
 749 middle 3 figures (b-d), and it is based on the “mitigation” emissions under G4, RCP4,5 and RCP8.5
 750 in the bottom 3 figures (e-g).

751

752 4. Discussion

753 4.1 Apparent temperature

754

755 Both ISIMIP and WRF can reproduce the observed (CN05.1) spatial patterns and
 756 seasonal variabilities of apparent temperature in the region around Beijing. WRF shows
 757 warm biases in AP during all months relative to CN05.1 due to warmer temperatures in
 758 urban areas, with the exception of BNU-ESM and HadGEM2-ES driven summers (Fig.
 759 [S&S13](#)). Both ISIMIP and WRF tend to overestimate population weighted NdAP₃₂ by

760 370% and 590%, respectively. These large discrepancies are due to relatively small
761 overestimates of the likelihood of the tails of the probability distributions which leads
762 to a dramatic increase in the frequency of extreme climate events (Dimri et al., 2018;
763 Huang et al., 2021). AP is about 1.5°C warmer than 2 m temperature over the Beijing
764 and Tianjin urban areas in summer due to higher vapor pressures amplifying warmer
765 urban temperatures, and this is despite humidity being lower over the cities. Under high
766 humidity conditions, a slight increase in temperature will cause a large increase in heat
767 stress (Li et al., 2018; Luo and Lau, 2019). AP is nearly 4°C colder than 2 m temperature
768 in winter due to wind speed (Fig. 2d). Differences between AP and 2 m temperature
769 (AP-T) during summer are greater in urban areas than neighboring rural areas.

770

771 The apparent temperatures in Beijing Tianjin urban areas under G4 in the 2060s are
772 simulated to be 1°C and 2.5°C lower than RCP4.5 and RCP8.5, although AP would be
773 higher than in the recent past. The cooling effect of G4 relative to RCP4.5 and RCP8.5
774 is greatest under HadGEM2-ES (Fig. S9S14, S10S15), due to the ESM having largest
775 temperature differences between scenarios (Wang et al., 2022). WRF downscaling
776 produces reduced seasonality in AP compared with ISIMIP, and WRF produces
777 relatively cooler summers and warmer winters than ISIMIP, and so much less
778 differences in apparent temperature ranges (Fig. 15). Differences in AP between G4 and
779 the RCP scenarios are mainly driven by temperature. In all scenarios and downscalings
780 AP rises faster than the temperature due to decreased wind speeds in the future (Li et
781 al., 2018; Zhu et al., 2021) but mainly because of rises in vapor pressure driven by
782 rising temperatures. This effect occurs despite the general drying expected under solar
783 geoengineering (Bala et al., 2008; Yu et al., 2015).

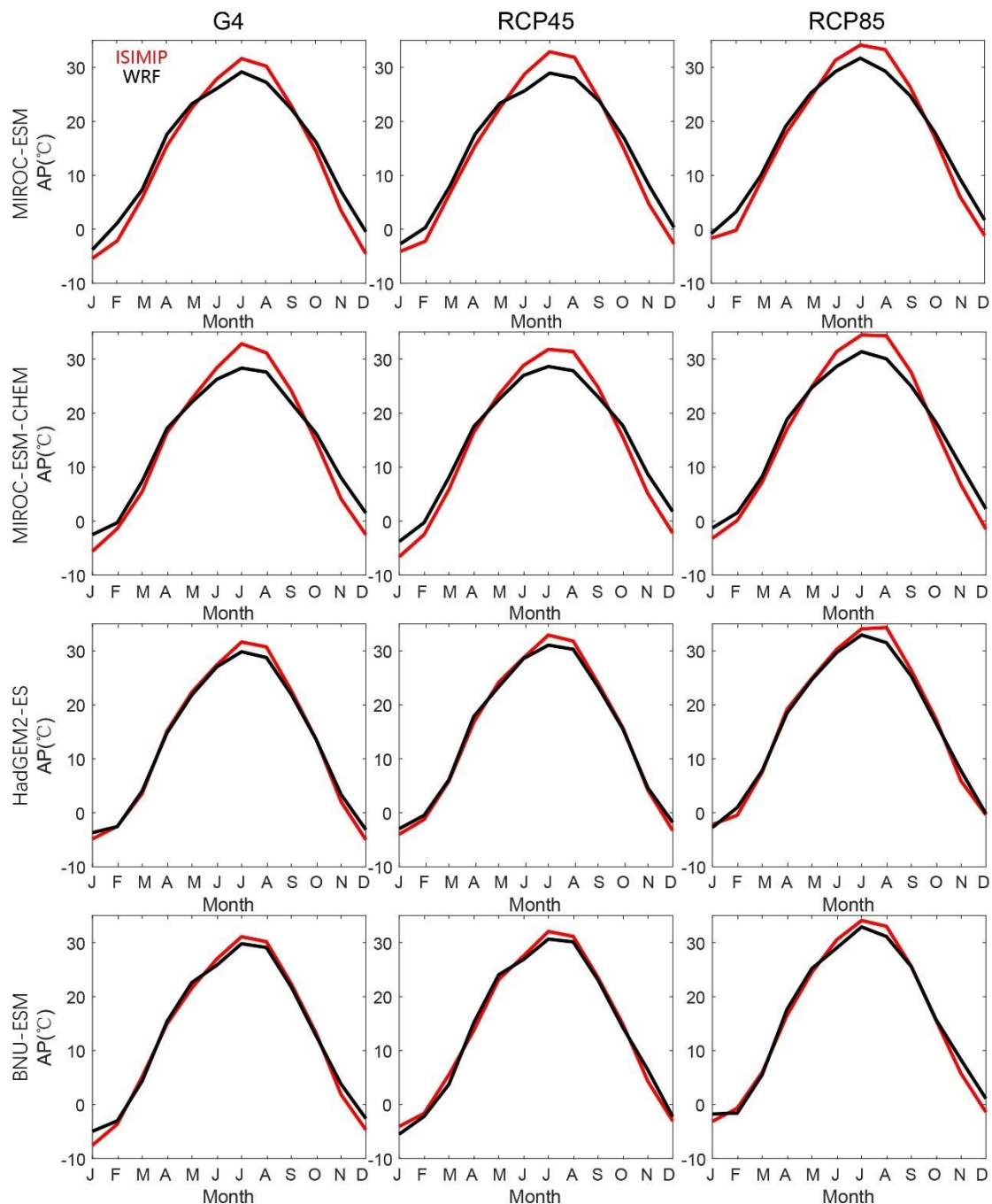
784

785 The NdAP_32 under G4 is projected to decrease by 8.6 days per year by ISIMIP and
786 6.3 days per year by WRF relative to RCP4.5 for Beijing-Tianjin Province. Much larger
787 reductions in NdAP_32 of 33.5 days per year (ISIMIP) and 19.6 days per year (WRF)
788 are projected relative to RCP8.5. Differences between scenarios in frequency of
789 dangerously hot days are far larger using ISIMIP statistical downscaling than using
790 WRF. This is another impact of the reduced seasonality of WRF compared with ISIMIP
791 (Fig. 15).

792

793 The higher resolution WRF simulation produces a much larger range of apparent
794 temperatures across the domain than CN05.1 and ISIMIP downscaling. This increased
795 variability makes reaching a statistical significance threshold more challenging for
796 WRF than ISIMIP results. Despite this, the ESM-driven differences in WRF output are
797 less than from ISIMIP, reflecting the physically based processes in the dynamic WRF
798 simulation. This reduces the impact of differences in ESM forcing at the domain
799 boundaries with WRF compared with the statistical bias correction and downscaling
800 methods. Although there are some uncertainties between models and downscaling
801 methods, G4 SAI can not only reduce the mean apparent temperature but also decrease
802 the probability of PDF tails (extreme events) in summer.

803



804
 805 **Figure 15.** Seasonal cycles of apparent temperature from MIROC-ESM, MIROC-ESM-CHEM,
 806 HadGEM2-ES and BNU-ESM under G4, RCP4.5 and RCP8.5 in Beijing-Tianjin urban areas during
 807 2060s based on ISIMIP (red) and WRF (black) methods.

808

809 **4.2 PM_{2.5}**

810 We established a set spatially gridded MLR models based on the 4 ESMs downscaled
 811 variables under ISIMIP and WRF. The meteorological factors impact PM_{2.5} in complex
 812 ways, but the simple spatially gridded MLR models display enough skill to make some
 813 illustrative projections of future PM_{2.5} explaining about 70% of the variance during the
 814 historical period. PM_{2.5} concentration is correlated with emissions and anti-correlated

815 with temperature in most parts of the domain (Fig. [S19S25-S20S26](#)). Increased
816 turbulence increases diffusion of PM_{2.5} (Yang et al., 2016), and higher temperatures
817 increase evaporation losses (Liu et al., 2015) of ammonium nitrate (Chuang et al., 2017),
818 and other components (Wang et al., 2006). Humidity may have both positive and
819 negative effects on PM_{2.5} (Chen et al., 2020). It causes more water vapor to adhere to
820 the surface of PM_{2.5}, thereby increasing its mass concentration and facilitating aerosol
821 growth (Cheng et al., 2017; Liao et al., 2017). However, when the humidity exceeds a
822 certain threshold, coagulation and particle mass increases rapidly, promoting deposition
823 (Li et al., 2015). So, the slope coefficients between PM_{2.5} and humidity are positive in
824 low humidity areas, including southern plain and the Beijing-Tianjin province, but
825 negative in some northern mountain areas (Fig. [S2519](#), [S20S26](#)).

826
827 There are large spatial differences in wind speed and direction impacts on PM_{2.5}. Yang
828 et al. (2016) found that weaker northerly and westerly winds tend to increase the PM_{2.5}
829 concentration in northern and eastern China, respectively. The effects of wind direction
830 depend on the distribution of emitted PM_{2.5} and the condition of the underlying surface
831 (Chen et al., 2020). Most sources of PM_{2.5} lie to the south of our domain, relatively
832 clean conditions prevail to the north, so northerly winds tend to advect clean air, while
833 southerlies bring high concentrations of aerosols. Weak winds tend to increase PM_{2.5}
834 and smog formation due to sinking air and weak diffusion (Su et al., 2017; Yang et al.,
835 2017).

836
837 Xu et al. (2021) projected 2030 PM_{2.5} concentrations will decrease by 8.8% and 5.5%
838 under RCP4.5 and RCP8.5 respectively relative to 2015. Wang et al. (2021) also
839 projected decreasing trends in China under RCP4.5 and RCP8.5 during 2030-2050.
840 There were seasonal changes in PM_{2.5} concentration differences between RCP4.5/8.5
841 scenarios and the historical scenario near the Bohai Sea (Dou et al., 2021). However,
842 there are also some simulations where PM_{2.5} concentrations increase in warmer climates.
843 Hong et al. (2019) suggest that annual mean PM_{2.5} concentrations will increase 1-8
844 µg/m³ in an area including Beijing and Tianjin under RCP4.5 during 2046-2050,
845 compared with 2006-2010. These inconsistent responses are mainly caused by the
846 differences in the selection of ESMs, chemical transport models and climate/emission
847 scenarios. Different RCP scenarios not only correspond to different future climate states,
848 but also have different anthropogenic emissions of air pollutants. In our study, we do
849 not consider the PM_{2.5} emission differences between RCP4.5 and RCP8.5, and instead
850 applied the ECLIPSE PM_{2.5} emission scenarios in our MLR projection.

851
852 Emissions reductions are expected to play the dominant role in the decrease of PM_{2.5}
853 concentrations under G4 aerosol “mitigation” in 2060s (Fig. 12). Meteorological
854 changes under the different future scenarios make much smaller changes as evidenced
855 by the scenarios using “baseline” – that is present day PM_{2.5} emissions, with decreases
856 in mean annual concentration of 1.0 (1.3), 1.8 (2.0), 3.3 (3.2) µg/m³ over Beijing-

857 Tianjin province under G4, RCP4.5 and RCP8.5 with WRF (ISIMIP), (Table S2S3),
858 which are mainly caused by the temperature increases (Fig. 13). The negative
859 relationships between emission and PM_{2.5} concentration result in the increase of PM_{2.5}
860 under G4 (“mitigation”) relative to 2010s in the north of Beijing with WRF. This may
861 be due to changes in PM_{2.5} out of the domain being opposite to those in domain during
862 the MLR fitting period, since relocation of polluting sources from the urban areas
863 mainly to the west, was occurring over the calibration period. The accuracy of PM_{2.5}
864 emission data is also crucial for training MLR models, and PM_{2.5} data was sparse before
865 2013, relying on reconstructions based on satellite optical depth estimates. Although
866 both increase of temperature and decrease of emission explain more than 90% of the
867 decrease in PM_{2.5} in most areas, there are large spatial differences due to wind and
868 humidity. On the one hand, there is uncertainty in the differences in changes of wind
869 speed and humidity between different ESMs and downscaling methods; on the other
870 hand, the complex physical relationship between them and PM_{2.5} also increases
871 uncertainties. Reductions in PM_{2.5} in the future are projected to decrease PM_{2.5} related
872 health issues, although its effect on different diseases are different. Changes in PM_{2.5}
873 related risk between G4 and RCPs are from 1-3%, with PM_{2.5} emissions policy
874 dominating differences over climate scenario.

875
876 There are some differences in projecting PM_{2.5} concentration between WRF and ISIMIP
877 methods. Compared to the 2010s reference, PM_{2.5} concentration in ISIMIP are
878 projected to decrease more than using WRF in G4 under the “mitigation” scenario
879 during the 2060s over the Tianjin province (Fig. 11a, e). However, the spatial patterns
880 of changes in PM_{2.5} concentration between G4 and RCP4.5/8.5 under the “mitigation”
881 scenario during 2060s are similar (Fig. 11c-d, g-h). This means that the effects of
882 different downscaled methods on projecting PM_{2.5} are small if we only consider the
883 climate change alone without considering emissions changes. Due to the larger
884 regression coefficient of emissions in the MLR under the ISIMIP method (Fig. S25,
885 S26), the negative changes in PM_{2.5} concentration are larger between “mitigation” and
886 baseline under G4 during 2060s than that under the WRF method. Correspondingly, the
887 ISIMIP method has a greater reduction in PM_{2.5} related RR than WRF under three future
888 climate scenarios during the 2060s.

889
890 Eastham et al. (2018) deduced from experiments using 1 Tg/yr SAI in a coupled
891 chemistry-transport model directly simulating atmospheric chemistry, transport,
892 radiative transfer of UV, emissions, and loss processes, that per unit mass emitted,
893 surface-level emissions of sulfate result in 25 times greater population exposure to
894 PM_{2.5} than emitting the same aerosol into the stratosphere. The G4 experiment specifies
895 5 Tg/yr injection rate, which over our domain would equate to 1450 t/yr if it was
896 deposited uniformly globally (which it certainly would not be). Reducing this by the
897 1/25 factor amounts to 58 t/yr which can be compared with present PM_{2.5} emissions of
898 around 3.3×10⁵ t/year in our domain. If we consider the aerosol deposition under G4
899 scenarios, PM_{2.5} concentration will be 0-1 µg/m³ higher than that without due to

900 deposition of the SAI aerosols (Fig. S21-S27), and RR is projected to increase by 0.01%
901 for Beijing-Tianjin province (Table S3-S4). This comparison suggests that tropospheric
902 emissions will be much more important for human health in our domain than from the
903 SAI specified by G4.

904
905 The most important change in PM_{2.5} will come from emissions reductions, with the
906 different weather conditions under both G4 and RCP scenarios making relatively little
907 practical differences in concentrations. PM_{2.5} concentration is expected to decrease
908 significantly (ISIMIP: ~~-6.57.6~~ μg/m³, WRF: ~~-4.35.4~~ μg/m³) in the Beijing-Tianjin
909 province, but they will still not meet either Chinese or international standards. The
910 temperature under G4 is lower than that under RCP4.5 and RCP8.5 scenarios, which
911 makes the PM_{2.5} concentration under G4 higher. But the difference in PM_{2.5} between
912 the two is small and even within uncertainty due to projected differences in humidity
913 and wind. Potentially improved estimates from more complex models such as WRF-
914 Chem, CMAQ and GEOS-Chem over the simple MLR methods used here will be of
915 limited value unless the differences between the ESM driving these models is reduced.
916 It can be confirmed that emission policies based on the 13th Five Year Plan are not
917 enough, and higher emission standards need to be developed for a healthy living
918 environment.

919
920 Our study did not consider the impacts of socio-economic pathways on PM_{2.5} future
921 emissions, instead we explore the meteorological differences between the SAI G4
922 scenario and the greenhouse gas RCP4.5/RCP8.5 on PM_{2.5} concentrations. PM_{2.5}
923 emissions were defined by the uncontrolled (“baseline”) and a scenario where
924 technological intervention (“mitigation”) reduces emissions. There are some limitations
925 in our study. Firstly, the HTAP_V3 dataset only includes anthropogenic PM_{2.5} emission,
926 not natural PM_{2.5} emission. Natural PM_{2.5} will also change in the future under changing
927 climate. The sources of natural PM_{2.5} include the sandstorms that sometimes occur in
928 spring as extreme winds mobilize dry unvegetated soils. These relatively extreme
929 conditions are difficult to simulate in ESM and subject to land use policy e.g., the
930 numerous ecosystem service measures undertaken by China over the last five decades
931 (Miao et al.,2015). Secondly, although PM_{2.5} concentration includes both primary and
932 secondary PM_{2.5} during model training, we do not consider the precursor gases for
933 secondary PM_{2.5} directly. The sensitivity of MLR may diminish at the high PM_{2.5} values
934 when secondary PM_{2.5} dominates the variability of total PM_{2.5} (Upadhyay et al., 2018).
935 Thirdly, we only consider the effect of dominant near-surface meteorological variables
936 on the PM_{2.5}. However, the vertical transport of pollutants related to vertical
937 atmospheric stability should not be ignored (Lo et al., 2006; Wu et al., 2005), and this
938 may contribute to the differences in RCP4.5 scenario from our MLR model and more
939 sophisticated simulations (Fig. S7). Finally, although it is insignificant for the Beijing
940 and Tianjin provinces, the MLR model suffers collinearity problems in some areas.
941 These factors play smaller roles as we are mainly considering changes in PM_{2.5}

942 concentration between different climate scenarios. Nevertheless, projection for changes
943 in PM_{2.5} between SAI scenarios and per greenhouse gas scenarios would be valuable
944 for global air quality impacts from geoengineering.

945

946 **5. Conclusion**

947 Our study on thermal comfort and aerosol pollution under geoengineering scenarios for
948 the Beijing megalopolis may be useful across the developing world, which is expected
949 to suffer disproportionate climate impact damages relative the global mean, while also
950 undergoing rapid urbanization. Assessing health impacts and mortality due to heat
951 stress and PM_{2.5} under greenhouse gas scenarios should consider urbanization and the
952 change to concrete surfaces from vegetation that leads to differences in heat capacities,
953 rates of evapotranspiration, and hence humidity and apparent temperature. These
954 require downscaled analyses, accurate meteorological and high-resolution land surface
955 datasets, and industrial development scenarios.

956

957 In our analysis we assumed the urban area did not change over time, and also that
958 population remains distributed as in the recent past. This may be reasonable in the
959 highly developed and relatively mature greater Beijing-Tianjin region but should be
960 considered in rapidly urbanizing regions elsewhere. There certainly will be changes
961 over time in the radiative cooling from surface pollution sources. PM_{2.5} is a health issue
962 in many developing regions (Ran et al., 2023), but as wealth increases efforts to curb
963 air pollution generally clean the air. This has clear health benefits, but also removes
964 aerosols from the troposphere that cool the surface. The urban areas that have higher
965 apparent temperatures at present are also the areas with greatest aerosol load and hence
966 greatest cooling. Once that is removed direct radiation, air temperatures and apparent
967 temperatures will all rise – by several degrees (Wang et al., 2016). So, a future more
968 comprehensive health impact study would include both the negative health impacts of
969 aerosol pollution and the potential cooling effects those aerosols produce. Additionally,
970 the formulation of apparent temperature used does not consider the effect of radiation
971 on human comfort (Kong and Huber, 2022). When PM_{2.5} levels are high there is no
972 shade because the sky is milky-white, similarly SAI will brighten the sky (Kravitz et
973 al., 2012). Comfort is increased in clear sky conditions when shade is readily found.

974

975 The changes simulated to relative risk from increased PM_{2.5} under the G4 SAI scenario
976 are about 1-3% worse than under RCP4.5, mainly because of lower temperatures under
977 G4. The difference this would make to the overall health burden under SAI depends on
978 the range of other impacts that include changes in apparent temperature we discuss. G4
979 reduces the number of days with AP>32 (when extreme caution is advised) by 6-8 per
980 year relative to RCP4.5 and by 20-34 relative to RCP8.5. But G4 itself will still increase
981 these extreme caution days by 1-20 relative to conditions in the 2010s. Lowering PM_{2.5}
982 emissions will increase ground temperatures and the associated risk of dangerous

983 apparent temperatures will also increase rapidly as the distribution of temperatures is
984 shifted making presently rare hot events into much more frequent heat waves.
985

986 **Code and data availability**

987 All ESM data used in this work are available from the Earth System Grid Federation
988 (WCRP, 2021; <https://esgf-node.llnl.gov/projects/cmip6>, last access: 14 July 2021).
989 The WRF and ISIMIP bias-corrected and downscaled results are available for the
990 authors on request. WRF and ISIMIP codes are freely available at the references cited
991 in the methods sections.

992 **Supplement link**

993 The link to the supplement will be included by Copernicus.

994 **Author contribution**

995 JCM and LZ designed the experiments, JW performed the simulations. All the authors
996 wrote the manuscript.

997 **Competing interests**

998 The authors declare that they have no conflict of interest.

999 **Disclaimer**

1000 Publisher's note: Copernicus Publications remains neutral with regard to jurisdictional
1001 claims in published maps and institutional affiliations.

1002 **Special issue statement:**

1003 This article is part of the special issue "Resolving uncertainties in solar geoengineering
1004 through multi-model and large-ensemble simulations (ACP/ESD inter-journal SI)". It
1005 is not associated with a conference.

1006 **Acknowledgements**

1007 We thank the editor and two constrictive referees for improving the manuscript. This
1008 work relies on the climate modeling groups participating in the Geoengineering Model
1009 Intercomparison Project and their model development teams; the CLIVAR/WCRP

1010 Working Group on Coupled Modeling for endorsing the GeoMIP; and the scientists
1011 managing the earth system grid data nodes who have assisted with making GeoMIP
1012 output available. This research was funded by the National Key Science Program for
1013 Global Change Research (2015CB953602).

1014
1015
1016
1017

1018 **References**

- 1019 Burnett, R., Pope III, C., Ezzati, M., Olives, C., Lim, S., Mehta, S., Shin, H., Singh, G.,
1020 Hubbell, B., Brauer, M., Anderson, A., Smith, K., Balmes, J., Bruce, N., Kan, H.,
1021 Laden, F., Prüss-Ustün, A., Turner, M., Gapstur, S., Diver, W., and Cohen, A.: An
1022 Integrated Risk Function for Estimating the Global Burden of Disease Attributable
1023 to Ambient Fine Particulate Matter Exposure, *Environ., Health Perspect.*, 122, 397-
1024 403, <https://doi.org/10.1289/ehp.1307049>, 2014.
- 1025 Bala, G., Duffy, P. B., Taylor, K. E.: Impact of geoengineering schemes on the global
1026 hydrological cycle, *Proc. Natl. Acad. Sci. USA*, 105 (22), 7664-7669,
1027 <https://doi.org/10.1073/pnas.0711648105>, 2008.
- 1028 [Chen, Z., Cai, J., Gao, B., Xu, B., Dai, S., He, B., Xie, X.: Detecting the causality
1029 influence of individual meteorological factors on local PM_{2.5} concentrations in the
1030 Jing-Jin-Ji region, *Sci. Rep.*, 7, 40735, <https://doi.org/10.1038/srep40735>, 2017.](#)
- 1031 Chen, Z., Chen, D., Kwan, M.-P., Chen, B., Gao, B., Zhuang, Y., Li, R., and Xu, B.: The
1032 control of anthropogenic emissions contributed to 80 % of the decrease in
1033 PM_{2.5} concentrations in Beijing from 2013 to 2017, *Atmos. Chem. Phys.*, 19, 13519–
1034 13533, <https://doi.org/10.5194/acp-19-13519-2019>, 2019.
- 1035 Chen, Z., Chen, D., Zhao, C., Kwan, M., Cai, J., Zhuang, Y., Zhao, B., Wang, X., Chen,
1036 B., Yang, J., Li, R., He, B., Gao, B., Wang, K., and Xu, B.: Influence of
1037 meteorological conditions on PM_{2.5} concentrations across China: A review of
1038 methodology and mechanism, *Environ. Int.*, 139, 105558,
1039 <https://doi.org/10.1016/j.envint.2020.105558>, 2020.
- 1040 Chen, Z., Xie, X., Cai, J., Chen, D., Gao, B., He, B., Cheng, N., and Xu, B.:
1041 Understanding meteorological influences on PM_{2.5} concentrations across China: a
1042 temporal and spatial perspective, *Atmos. Chem. Phys.*, 18, 5343–5358,
1043 <https://doi.org/10.5194/acp-18-5343-2018>, 2018.
- 1044 Cheng, L., Meng, F., Chen, L., Jiang, T., and Su, L.: Effects on the haze pollution from
1045 autumn crop residue burning over the Jing-Jin-Ji Region, *China Environ. Sci.*, 37,
1046 2801–2812, 2017.
- 1047 Chi, X., Li, R., Cubasch, U., Cao, W.: The thermal comfort and its changes in the 31
1048 provincial capital cities of mainland China in the past 30 years, *Theor. Appl.*
1049 *Climatol.*, 132(1-2), 599–619, 2018.
- 1050 Chuang, M., Chou, C., Lin, N., Takami, A., Hsiao, T., Lin, T., Fu, J., Pani, S., Lu, Y., and
1051 Yang, T.: A simulation study on PM_{2.5} sources and meteorological characteristics at

1052 the northern tip of Taiwan in the early stage of the Asian haze period, *Aerosol Air*
1053 *Qual. Res.*, 17, 3166-3178, <https://doi.org/10.4209/aaqr.2017.05.0185>, 2017.

1054 Collins, W. J., Bellouin, N., Doutriaux-Boucher, M., Gedney, N., Halloran, P., Hinton,
1055 T., Hughes, J., Jones, C. D., Joshi, M., Liddicoat, S., Martin, G., O'Connor, F., Rae,
1056 J., Senior, C., Sitch, S., Totterdell, I., Wiltshire, A., Woodward, S.: Development
1057 and evaluation of an Earth-System model – HadGEM2, *Geosci. Model Dev.*, 4,
1058 1051–1075, <https://doi.org/10.5194/gmd-4-1051-2011>, 2011.

1059 Curry, C. L., Sillmann, J., Bronaugh, D., Alterskjaer, K., Cole, J. N. S., Ji, D., Kravitz,
1060 B., Kristjánsson, J. E., Moore, J. C., Muri, H., Niemeier, U., Robock, A., Tilmes, S.,
1061 and Yang, S.: A multimodel examination of climate extremes in an idealized
1062 geoengineering experiment, *J. Geophys. Res.-Atmos.*, 119, 3900–3923,
1063 <https://doi.org/10.1002/2013JD020648>, 2014.

1064 Dimri, A. P., Kumar, D., Choudhary, A., Maharana, P.: Future changes over the
1065 Himalayas: Maximum and minimum temperature, *Global and Planetary Change*,
1066 162, 212-234, <https://doi.org/10.1016/j.gloplacha.2018.01.015>, 2018.

1067 [Dou, C., Ji, Z., Xiao, Y., Zhu, X., and Dong, W.: Projections of air pollution in northern](https://doi.org/10.3390/rs13163064)
1068 [China in the two RCPs scenarios, *Remote Sens.*, 13, 3064,](https://doi.org/10.3390/rs13163064)
1069 <https://doi.org/10.3390/rs13163064>, 2021.

1070 Eastham, D., Weisenstein, D., Keith, D., and Barrett, A.: Quantifying the impact of
1071 sulfate geoengineering on mortality from air quality and UV-B exposure, *Atmos.*
1072 *Environ.*, 187, 424–434. DOI: <http://dx.doi.org/10.1016/j.atmosenv.2018.05.047>,
1073 2018.

1074 Fan, M., Zhang, Y., Lin, Y., Cao, F., Sun, Y., Qiu, Y., Xing, G., Dao, X., and Fu, P.:
1075 Specific sources of health risks induced by metallic elements in PM_{2.5} during the
1076 wintertime in Beijing, China, *Atmos. Environ.*, 246, 118112,
1077 <https://doi.org/10.1016/j.atmosenv.2020.118112>, 2021.

1078 Fischer, E., and Knutti, R.: Robust projections of combined humidity and temperature
1079 extremes, *Nat. Clim. Change*, 3, 126-130, <https://doi.org/10.1038/nclimate1682>,
1080 2013.

1081 [Foley, K. M., Roselle, S. J., Appel, K. W., Bhave, P. V., Pleim, J. E., Otte, T. L., Mathur,](https://doi.org/10.5194/gmd-3-205-2010)
1082 [R., Sarwar, G., Young, J. O., Gilliam, R. C., Nolte, C. G., Kelly, J. T., Gilliland, A.](https://doi.org/10.5194/gmd-3-205-2010)
1083 [B., and Bash, J. O.: Incremental testing of the Community Multiscale Air Quality](https://doi.org/10.5194/gmd-3-205-2010)
1084 [\(CMAQ\) modeling system version 4.7, *Geosci. Model Dev.*, 3, 205–226,](https://doi.org/10.5194/gmd-3-205-2010)
1085 <https://doi.org/10.5194/gmd-3-205-2010>, 2010.

1086 Fu, J., Jiang, D., Huang, Y.: 1 km Grid Population Dataset of China, *Digital Journal of*
1087 *Global Change Data Repository*, <https://doi.org/10.3974/geodb.2014.01.06.V1>,
1088 2014.

1089 Garcia, F. C., Bestion, E., Warfield, R., Yvon-Durocher, G.: Changes in temperature alter
1090 the relationship between biodiversity and ecosystem functioning, *Proc. Natl. Acad.*
1091 *Sci. U.S.A.*, 115, 10989–10999, <https://doi.org/10.1073/pnas.1805518115>, 2018.

1092 Grinsted, A., Moore, J., and Jevrejeva, S.: Projected Atlantic tropical cyclone threat from
1093 rising temperatures, *PNAS*, 110, 5369-5373, <https://doi/10.1073/pnas.1209980110>,
1094 2013.

1095 Grundstein, A. and Dowd, J.: Trends in extreme apparent temperatures over the United
1096 States, 1949-2010, *J. Appl. Meteorol. Climatol.*, 50(8), 1650–1653,
1097 <https://doi.org/10.1175/JAMC-D-11-063.1>, 2011.

1098 Guan, W., Zheng, X., Chung, K., and Zhong, N.: Impact of air pollution on the burden
1099 of chronic respiratory diseases in China: time for urgent action, *Lancet*, 388, 1939-
1100 1951, [https://doi.org/10.1016/S0140-6736\(16\)31597-5](https://doi.org/10.1016/S0140-6736(16)31597-5), 2016.

1101 [Guo, L., Zhang, Y., Lin, H., Zeng, W., Liu, T., Xiao, J., Rutherford, S., You, J., Ma, W.:
1102 The washout effects of rainfall on atmospheric particulate pollution in two Chinese
1103 cities, *Environ. Pollut.*, 215, 195-202, <https://doi.org/10.1016/j.envpol.2016.05.003>,
1104 2016.](#)

1105 Han, J., Wang, J., Zhao, Y., Wang, Q., Zhang, B., Li, H., and Zhai, J.: Spatio-temporal
1106 variation of potential evapotranspiration and climatic drivers in the Jing-Jin-Ji region,
1107 North China, *Agric. For. Meteorol.*, 256, 75-83,
1108 <https://doi.org/10.1016/j.agrformet.2018.03.002>, 2018.

1109 Hempel, S., Frieler, K., Warszawski, L., Schewe, J., and Piontek, F.: A trend-preserving
1110 bias correction – the ISI-MIP approach, *Earth Syst. Dynam.*, 4, 219–236,
1111 <https://doi.org/10.5194/esd-4-219-2013>, 2013.

1112 Hersbach, H., Bell, B., Berrisford, P., Biavati, G., Horányi, A., Muñoz Sabater, J.,
1113 Nicolas, J., Peubey, C., Radu, R., Rozum, I., Schepers, D., Simmons, A., Soci, C.,
1114 Dee, D., Thépaut, J-N.: ERA5 hourly data on pressure levels from 1979 to present,
1115 Copernicus Climate Change Service (C3S) Climate Data Store (CDS),
1116 <https://doi.org/10.24381/cds.bd0915c6>, 2018.

1117 Ho, H. C., Knudby, A., Xu, Y., Hodul, M., Aminipouri, M.: A comparison of urban heat
1118 islands mapped using skin temperature, air temperature, and apparent temperature
1119 (Humidex), for the greater Vancouver area, *Science of The Total Environment*, 544,
1120 929-938, <https://doi.org/10.1016/j.scitotenv.2015.12.021>, 2016.

1121 [Hong, C., Zhang, Q., Zhang, Y., Davis, S., Tong, D., Zheng, Y., Liu, Z., Guan, D., He,
1122 K., and Schellnhuber, H. J.: Impacts of climate change on future air quality and
1123 human health in China, *PNAS*, 116, 17193-17200,
1124 <https://doi.org/10.1073/pnas.1812881116>, 2019.](#)

1125 Huang, J., Li, Q., Song, Z.: Historical global land surface air apparent temperature and
1126 its future changes based on CMIP6 projections, *Science of The Total Environment*,
1127 816, 151656, <https://doi.org/10.1016/j.scitotenv.2021.151656>, 2021.

1128 IPCC, 2021. Climate change 2021: the physical science basis. In: Masson-Delmotte, V.,
1129 Zhai, P., Pirani, A., Connors, S.L., Péan, C., Berger, S., Caud, N., Chen, Y., Goldfarb,
1130 L., Gomis, M.I., Huang, M., Leitzell, K., Lonnoy, E., Matthews, J.B.R., Maycock,
1131 T.K., Waterfiel, T., Yelekçi, O., Yu, R., B.Z. (Eds.), Contribution of Working
1132 Group I to the Sixth Assessment Report of the Intergovernmental Panel on Climate
1133 Change. Cambridge University Press In Press.

1134 Jacobs, S. J., Pezza, A. B., Barras, V., Bye, J., Vihma, T.: An analysis of the
1135 meteorological variables leading to apparent temperature in Australia: present
1136 climate, trends, and global warming simulations, *Glob. Planet. Chang.*, 107, 145–
1137 156, 2013.

1138 Janssens-Maenhout, G., Crippa, M., Guizzardi, D., Dentener, F., Muntean, M., Pouliot,
1139 G., Keating, T., Zhang, Q., Kurokawa, J., Wankmüller, R., Denier van der Gon, H.,
1140 Kuenen, J. J. P., Klimont, Z., Frost, G., Darras, S., Koffi, B., and Li, M.: HTAP_v2.2:
1141 a mosaic of regional and global emission grid maps for 2008 and 2010 to study
1142 hemispheric transport of air pollution, *Atmos. Chem. Phys.*, 15, 11411-11432,
1143 <https://doi.org/10.5194/acp-15-11411-2015>, 2015.

1144 Ji, D., Fang, S., Curry, C. L., Kashimura, H., Watanabe, S., Cole, J. N. S., Lenton, A.,
1145 Muri, H., Kravita, B., Moore, J. C.: Extreme temperature and precipitation response
1146 to solar dimming and stratospheric aerosol geoengineering, *Atmospheric Chemistry
1147 and Physics*, 18, 10133-10156, <https://doi.org/10.5194/acp-18-10133-2018>, 2018.

1148 Ji, D., Wang, L., Feng, J., Wu, Q., Cheng, H., Zhang, Q., Yang, J., Dong, W., Dai, Y.,
1149 Gong, D., Zhang, R.-H., Wang, X., Liu, J., Moore, J. C., Chen, D., and Zhou, M.:
1150 Description and basic evaluation of Beijing Normal University Earth System Model
1151 (BNU-ESM) version 1, *Geosci. Model Dev.*, 7, 2039–2064,
1152 <https://doi.org/10.5194/gmd-7-2039-2014>, 2014.

1153 Jin, H., Chen, X., Zhong, R., and Liu, M.: Influence and prediction of PM_{2.5} through
1154 multiple environmental variables in China, *Sci. Total Environ.*, 849, 157910,
1155 <https://doi.org/10.1016/j.scitotenv.2022.157910>, 2022.

1156 Jones, A. C., Hawcroft, M. K., Haywood, J. M., Jones, A., Guo, X., Moore, J.C.:
1157 Regional climate impacts of stabilizing global warming at 1.5 K using solar
1158 geoengineering, *Earth's Future*, 6, <https://doi.org/10.1002/2017EF000720>, 2018.

1159 Kim, D. H., Shin, H. J., Chung, I. U.: Geoengineering: Impact of marine cloud
1160 brightening control on the extreme temperature change over East Asia, *Atmosphere*,
1161 11(12), 1345, <https://doi.org/10.3390/atmos11121345>, 2020.

1162 Klimont, Z., Kupiainen, K., Heyes, C., Purohit, P., Cofala, J., Rafaj, P., Borken-Kleefeld,
1163 J., and Schöpp, W.: Global anthropogenic emissions of particulate matter including
1164 black carbon, *Atmos. Chem. Phys.*, 17, 8681–8723, <https://doi.org/10.5194/acp-17-8681-2017>, 2017.

1166 Kong, Q., and Huber, M.: Explicit calculations of wet-bulb globe temperature compared
1167 with approximations and why it matters for labor productivity, *Earth's Future*, 10,
1168 e2021EF002334, <https://doi.org/10.1029/2021EF002334>, 2022.

1169

1170 Kraaijenbrink, P. D. A., Bierkens, M. F. P., Lutz A. F., Immerzeel, W. W.: Impact of a
1171 global temperature rise of 1.5 degrees Celsius on Asia's glaciers, *Nature*, 549, 257-
1172 260, <https://doi.org/10.1038/nature23878>, 2017.

1173 Kravitz, B., MacMartin, D., and Caldeira, K.: Geoengineering: Whiter skies?, *Geophys.
1174 Res. Lett.*, 39, L11801, <https://doi.org/10.1029/2012GL051652>, 2012.

1175 Kravitz, B., Robock, A., Boucher, O., Schmidt, H., Taylor, K. E., Stenchikov, G., and
1176 Schulz, M.: The geoengineering model intercomparison project (GeoMIP), *Atmos.
1177 Sci. Lett.*, 12(2), 162-167, <https://doi.org/10.1002/asl.316>, 2011.

1178 Kuswanto, H., Kravitz, B., Miftahurrohman, B., Fauzi, F., Sopahaluwaken, A., and
1179 Moore, J. C.: Impact of solar geoengineering on temperatures over the Indonesian
1180 Maritime Continent, *Int. J. Climatol.*, 1-20, <https://doi.org/10.1002/joc.7391>, 2021.

1181 Lee, C. and Sheridan, S.: A new approach to modeling temperature-related mortality:

1182 non-linear autoregressive models with exogenous input, *Environ. Res.*, 164:53–64,
 1183 <https://doi.org/10.1016/j.envres.2018.02.020>, 2018.

1184 Lenton, T. and Vaughan, N.: The radiative forcing potential of different climate
 1185 geoengineering options, *Atmos. Chem. Phys.*, 9, 5539–5561,
 1186 <https://doi.org/10.5194/acp-9-5539-2009>, 2009.

1187 Li, D., Wu, Q., Feng, J., Wang, Y., Wang, L., Xu, Q., Sun, Y., Cao, K., and Cheng, H.:
 1188 The influence of anthropogenic emissions on air quality in Beijing-Tianjin-Hebei of
 1189 China around 2050 under the future climate scenario, *J. Cleaner Prod.*, 388, 135927,
 1190 <https://doi.org/10.1016/j.jclepro.2023.135927>, 2023.

1191 Li, J., Chen, H., Li, Z., Wang, P., Cribb, M., and Fan, X.: Low-level temperature
 1192 inversions and their effect on aerosol condensation nuclei concentrations under
 1193 different large-scale synoptic circulations, *Adv. Atmos. Sci.*, 32, 898-908,
 1194 <https://doi.org/10.1007/s00376-014-4150-z>, 2015.

1195 Li, J., Chen, Y., Gan, T., Lau, N.: Elevated increases in human-perceived temperature
 1196 under climate warming, *Nat. Clim. Chang.*, 8 (1), 43–47,
 1197 <https://doi.org/10.1038/s41558-017-0036-2>, 2018.

1198 Li, K., Liao, H., Zhu, J., and Moch, J.: Implications of RCP emissions on future PM_{2.5}
 1199 air quality and direct radiative forcing over China, *J. Geophys. Res. Atmos.*, 121, 12,
 1200 985-13, 008, <https://doi.org/10.1002/2016JD025623>, 2016.

1201 Li, M., Klimont, Z., Zhang, Q., Martin, R. V., Zheng, B., Heyes, C., Cofala, J., Zhang,
 1202 Y., and He, K.: Comparison and evaluation of anthropogenic emissions of SO₂ and
 1203 NO_x over China, *Atmos. Chem. Phys.*, 18, 3433–3456, <https://doi.org/10.5194/acp-18-3433-2018>, 2018.

1205 Liao, T., Wang, S., Ai, J., Gui, K., Duan, B., Zhao, Q., Zhang, X., Jiang, W., and Sun, Y.:
 1206 Heavy pollution episodes, transport pathways and potential sources of PM_{2.5} during
 1207 the winter of 2013 in Chengdu (China), *Sci. Total Environ.*, 584–585, 1056–1065,
 1208 <https://doi.org/10.1016/j.scitotenv.2017.01.160>, 2017.

1209 Lin, G., Fu, J., Jiang, D., Wang, J., Wang, Q., and Dong, D.: Spatial variation of the
 1210 relationship between PM_{2.5} concentrations and meteorological parameters in China,
 1211 *BioMed Res. Int.*, 2015, 684618, <https://doi.org/10.1155/2015/684618>, 2015.

1212 [Lo, J., Lau, A., Fung, J., and Chen, F.: Investigation of enhanced cross-city transport and](#)
 1213 [trapping of air pollutants by coastal and urban land-sea breeze circulations, *J.*](#)
 1214 [*Geophys. Res.-Atmos.*, 111\(D14\), <https://doi.org/10.1029/2005JD006837>, 2006.](#)

1215 Luo, M., & Lau, N.-C.: Characteristics of summer heat stress in China during 1979–2014:
 1216 Climatology and long-term trends, *Climate Dynamics*, 53(9), 5375–5388,
 1217 <https://doi.org/10.1007/s00382-019-04871-5>, 2019.

1218 Luo, M. and Lau, N.: Increasing Human-Perceived Heat Stress Risks Exacerbated by
 1219 Urbanization in China: A Comparative Study Based on Multiple Metrics, *Earth's*
 1220 *Future*, 9 (7), <https://doi.org/10.1029/2020EF001848>, 2021.

1221 Lyon, B. and Barnston, A.: Diverse characteristics of US summer heat waves, *J. Clim.*,
 1222 30 (19), 7827–7845, <https://doi.org/10.1175/JCLI-D-17-0098.1>, 2017.

1223 Maji, K., Ye, W., Arora, M., and Nagendra, S.: PM_{2.5}-related health and economic loss
 1224 assessment for 338 Chinese cities, *Environ. Int.*, 121, 392-403,
 1225 <https://doi.org/10.1016/j.envint.2018.09.024>, 2018.

- 1226 Matthews, T., Wilby, R., and Murphy, C.: Communicating the deadly consequences of
 1227 global warming for human heat stress, *PNAS*, 114, 3861-3866,
 1228 <https://doi.org/10.1073/pnas.1617526114>, 2017.
- 1229 [Miao, L., Moore, J. C., Zeng, F., Lei, J., Ding, J., He, B., and Cui, X.: Footprint of](#)
 1230 [research in desertification management in China, *Land Degrad. Dev.*, 26, 450-457,](#)
 1231 <https://doi.org/10.1002/ldr.2399>, 2015.
- 1232 Mishra, D., Goyal, P., and Upadhyay, A.: Artificial intelligence based approach to
 1233 forecast PM_{2.5} during haze episodes: a case study of Delhi, India, *Atmos. Environ.*,
 1234 102, 239–248, <https://doi.org/10.1016/j.atmosenv.2014.11.050>, 2015.
- 1235 Murray, F.: On the computation of saturation vapor pressure, Rand Corp Santa Monica
 1236 Calif, 1966.
- 1237 Nguyen, G., Shimadera, H., Uranishi, K., Matsuo, T., and Kondo, A.: Numerical
 1238 assessment of PM_{2.5} and O₃ air quality in Continental Southeast Asia: Impacts of
 1239 future projected anthropogenic emission change and its impacts in combination with
 1240 potential future climate change impacts, *Atmos. Environ.*, 226, 117398,
 1241 <https://doi.org/10.1016/j.atmosenv.2020.117398>, 2020.
- 1242 Perkins, S. and Alexander, L.: On the measurement of heat waves, *J Clim.*, 26 (13),
 1243 4500–4517, <https://doi.org/10.1175/JCLI-D-12-00383.1>, 2013.
- 1244 Ran, Q., Lee, S., Zheng, D., Chen, H., Yang, S., Moore, J., Dong, W.: Potential Health
 1245 and Economic Impacts of Shifting Manufacturing from China to Indonesia or India,
 1246 *Science of the total environment*, 855, 158634,
 1247 <http://dx.doi.org/10.1016/j.scitotenv.2022.158634>, 2022.
- 1248 Riahi, K., Rao, S., Krey, V., Cho, C., Chirkov, V., Fischer, G., Kindermann, G.,
 1249 Nakicenovic, N., Rafaj, P.: RCP 8.5—A scenario of comparatively high greenhouse
 1250 gas emissions, *Climatic Change* 109, 33, <https://doi.org/10.1007/s10584-011-0149->
 1251 [y](https://doi.org/10.1007/s10584-011-0149-y), 2011.
- 1252 Robock, A., Marquardt, A., Kravitz, B. and Stenchikov, G.: Benefits, risks, and costs of
 1253 stratospheric geoengineering, *Geophys. Res. Lett.*, 36(19),
 1254 <https://doi.org/10.1029/2009GL039209>, 2009.
- 1255 Shepherd, J.: Geoengineering the climate: Science, governance, and uncertainty, Royal
 1256 Society Policy document 10/09, 82 pp, 2009.
- 1257 Song, F., Zhang, G., Ramanathan, V. and Ruby Leung, L.: Trends in surface equivalent
 1258 potential temperature: A more comprehensive metric for global warming and
 1259 weather extremes, *Proc. Natl. Acad. Sci. U.S.A.*, 119, 6,
 1260 <https://doi.org/10.1073/pnas.2117832119>, 2022.
- 1261 Steadman, R. G.: A universal scale of apparent temperature, *J. Appl. Meteorol.*, 23 (12),
 1262 1674–1687, [https://doi.org/10.1175/1520-0450\(1984\)023<1674:AUSOAT>2.](https://doi.org/10.1175/1520-0450(1984)023<1674:AUSOAT>2.)
 1263 [O.CO;2](https://doi.org/10.1175/1520-0450(1984)023<1674:AUSOAT>2.O.CO;2), 1984.
- 1264 Steadman, R. G.: Norms of apparent temperature in Australia, *Aust. Meteorol. Mag.*, 43,
 1265 1–16, 1994.
- 1266 Stohl, A., Aamaas, B., Amann, M., Baker, L. H., Bellouin, N., Berntsen, T. K., Boucher,
 1267 O., Cherian, R., Collins, W., Daskalakis, N., Dusinska, M., Eckhardt, S., Fuglestvedt,
 1268 J. S., Harju, M., Heyes, C., Hodnebrog, Ø., Hao, J., Im, U., Kanakidou, M., Klimont,
 1269 Z., Kupiainen, K., Law, K. S., Lund, M. T., Maas, R., MacIntosh, C. R., Myhre, G.,

1270 Myriokefalitakis, S., Olivie, D., Quaas, J., Quennehen, B., Raut, J.-C., Rumbold, S.
1271 T., Samset, B. H., Schulz, M., Seland, Ø., Shine, K. P., Skeie, R. B., Wang, S., Yttri,
1272 K. E., and Zhu, T.: Evaluating the climate and air quality impacts of short-lived
1273 pollutants, *Atmos. Chem. Phys.*, 15, 10529–10566, [https://doi.org/10.5194/acp-15-](https://doi.org/10.5194/acp-15-10529-2015)
1274 10529-2015, 2015.

1275 Su, J., Brauer, M., Ainslie, B., Steyn, D., Larson, T., and Buzzelli, M.: An innovative land
1276 use regression model incorporating meteorology for exposure analysis, *Sci. Total*
1277 *Environ.*, 390, 520-529, <https://doi.org/10.1016/j.scitotenv.2007.10.032>, 2008.

1278 Tong, C., Yim, S., Rothenberg, D., Wang, C., Lin, C., Chen, Y., and Lau, N.: Projecting
1279 the impacts of atmospheric conditions under climate change on air quality over the
1280 Pearl River Delta region, *Atmos. Environ.*, 193, 79-87,
1281 <https://doi.org/10.1016/j.atmosenv.2018.08.053>, 2018.

1282 Torma, C. and Giogi, F.: Assessing the contribution of different factors in regional
1283 climate model projections using the factor separation method, *Atmos. Sci. Lett.*, 15,
1284 239–244, <https://doi.org/10.1002/asl2.491>, 2014.

1285 Upadhyay, A., Dey, S., Goyal, P., and Dash, S.: Projection of near-future anthropogenic
1286 PM_{2.5} over India using statistical approach, *Atmos. Environ.*, 186, 178-188,
1287 <https://doi.org/10.1016/j.atmosenv.2018.05.025>, 2018.

1288 Vandyck, T., Keramidas, K., Saveyn, B., et al.: A global stocktake of the Paris pledges:
1289 Implications for energy systems and economy, *Global Environmental Change*, 41,
1290 46-63, <https://doi.org/10.1016/j.gloenvcha.2016.08.006>, 2016.

1291 Wang, J., Allen, D., Pickering, K., Li, Z., He, H.: Impact of aerosol direct effect on East
1292 Asian air quality during the EAST-AIRE campaign, *J. Geophys. Res.- Atmos.*, 121,
1293 6534-6554, <https://doi.org/10.1002/2016JD025108>, 2016.

1294 Wang, J., Moore, J. C., Zhao, L., Yue, C., and Di, Z.: Regional dynamical and statistical
1295 downscaling temperature, humidity and windspeed for the Beijing region under
1296 stratospheric aerosol injection geoengineering, *Earth Syst. Dynam.*,
1297 <https://doi.org/10.5194/esd-2022-35>, 2022.

1298 Wang, J., Feng, J., Yan, Z., Hu, Y., and Jia, G.: Nested high-resolution modeling of the
1299 impact of urbanization on regional climate in three vast urban agglomerations in
1300 China, *J. Geophys. Res.- Atmos.*, 117(D21), <https://doi.org/10.1029/2012JD018226>,
1301 2017.

1302 Wang, J., Zhang, L., Niu, X., and Liu, Z.: Effects of PM_{2.5} on health and economic loss:
1303 Evidence from Beijing-Tianjin-Hebei region of China, *J. Cleaner Prod.*, 257, 120605,
1304 <https://doi.org/10.1016/j.jclepro.2020.120605>, 2020.

1305 Wang, P., Luo, M., Liao, W., Xu, Y., Wu, S., Tong, X., Tian, H., Xu, F., Han, Y.:
1306 Urbanization contribution to human perceived temperature changes in major urban
1307 agglomerations of China, *Urban Climate*, 38, 100910,
1308 <https://doi.org/10.1016/j.uclim.2021.100910>, 2021.

1309 Wang, S., Ancell, B., Huang, G., Baetz, B.: Improving robustness of hydrologic
1310 ensemble predictions through probabilistic pre- and post-processing in sequential
1311 data assimilation, *Water Resources Research*, 54, 2129–2151,
1312 <https://doi.org/10.1002/2018WR022546>, 2018.

- 1313 Wang, X., Huang, G., Lin, Q., Nie, X., Cheng, G., Fan, Y., Li, Z., Yao, Y., Suo, M.: A
 1314 stepwise cluster analysis approach for downscaled climate projection - a Canadian
 1315 case study, *Environ. Model Softw.*, 49, 141–151,
 1316 <https://doi.org/10.1016/j.envsoft.2013.08.006>, 2013.
- 1317 Wang, Y., Hu, J., Zhu, J., Li, J., Qin, M., Liao, H., Chen, K., and Wang, M.: Health
 1318 Burden and economic impacts attributed to PM_{2.5} and O₃ in China from 2010 to 2050
 1319 under different representative concentration pathway scenarios, *Resour. Conserv.*
 1320 *Recy.*, 173, 105731, <https://doi.org/10.1016/j.resconrec.2021.105731>, 2021.
- 1321 Wang, Y., Chen, L., Song, Z., Huang, Z., Ge, E., Lin, L., Luo, M.: Human-perceived-
 1322 temperature changes over South China: long-term trends and urbanization effects,
 1323 *Atmos. Res.*, 215, 116–127, <https://doi.org/10.1016/j.atmosres.2018.09.006>, 2019.
- 1324 Wang, Y., Yao, L., Wang, L., Liu, Z., Ji, D., Tang, G., Zhang, J., Sun, Y., Hu, N., and Xin,
 1325 J.: Mechanism for the formation of the January 2013 heavy haze pollution episode
 1326 over central and eastern China, *Sci. China Earth Sci.*, 57, 14–25,
 1327 <https://doi.org/10.1007/s11430-013-4773-4>, 2014.
- 1328 Wang, Y., Zhuang, G., Zhang, X., Huang, K., Xu, C., Tang, A., Chen, J., and An, Z.: The
 1329 ion chemistry, seasonal cycle, and sources of PM_{2.5} and TSP aerosol in Shanghai,
 1330 *Atmos. Environ.*, 40, 2935–2952, <https://doi.org/10.1016/j.atmosenv.2005.12.051>,
 1331 2006.
- 1332 Watanabe, S., Hajima, T., Sudo, K., Nagashima, T., Takemura, T., Okajima, H., Nozawa,
 1333 T., Kawase, H., Abe, M., Yokohata, T., Ise, T., Sato, H., Kato, E., Takata, K., Emori,
 1334 S., and Kawamiya, M.: MIROC-ESM 2010: model description and basic results of
 1335 CMIP5-20c3m experiments, *Geosci. Model Dev.*, 4, 845–872,
 1336 <https://doi.org/10.5194/gmd-4-845-2011>, 2011.
- 1337 Wei, J., Li, Z., Lyapustin, A., Sun, L., Peng, Y., Xue, W., Su, T., and Cribb, M.:
 1338 Reconstructing 1-km-resolution high-quality PM_{2.5} data records from 2000 to 2018
 1339 in China: spatiotemporal variations and policy implications, *Remote Sens. Environ.*,
 1340 252, 112136, <https://doi.org/10.1016/j.rse.2020.112136>, 2021.
- 1341 Wilcke, R. A. I., Mendlik, T., Gobiet, A.: Multi-variable error correction of regional
 1342 climate models, *Clim. chang.*, 120(4), 871–887, <https://doi.org/10.1007/s10584-013-0845-x>, 2013.
- 1344 Wu, D., Tie, X., Li, C., Ying, Z., Kai-Hon Lau, A., Huang, J., Deng, X., and Bi, X.: An
 1345 extremely low visibility event over the Guangzhou region: a case study, *Atmos.*
 1346 *Environ.*, 39, 6568–6577, <https://doi.org/10.1016/j.atmosenv.2005.07.061>, 2005.
- 1347 Wu, J., Gao, X., Giorgi, F., Chen, D.: Changes of effective temperature and cold/hot days
 1348 in late decades over China based on a high resolution gridded observation dataset,
 1349 *Int. J. Climatol.*, 37:788–800, <https://doi.org/10.1002/joc.5038>, 2017.
- 1350 Xu, J., Yao, M., Wu, W., Qiao, X., Zhang, H., Wang, P., Yang, X., Zhao, X., and Zhang,
 1351 J.: Estimation of ambient PM_{2.5}-related mortality burden in China by 2030 under
 1352 climate and population change scenarios: A modeling study, *Environ. Int.*,
 1353 156,106733, <https://doi.org/10.1016/j.envint.2021.106733>, 2021.
- 1354 Wu, J., Gao, X., Giorgi, F., Chen, D.: Changes of effective temperature and cold/hot days
 1355 in late decades over China based on a high resolution gridded observation dataset,
 1356 *Int. J. Climatol.*, 37:788–800, <https://doi.org/10.1002/joc.5038>, 2017.

- 1357 Xue, W., Zhang, J., Zhong, C., Li, X., and Wei, J.: Spatiotemporal PM_{2.5} variations and
1358 its response to the industrial structure from 2000 to 2018 in the Beijing-Tianjin-
1359 Hebei region, *J. Cleaner Prod.*, 279, 123742,
1360 <https://doi.org/10.1016/j.jclepro.2020.123742>, 2021.
- 1361 Yang, S., Ma, Y., Duan, F., He, K., Wang, L., Wei, Z., Zhu, L., Ma, T., Li, H., Ye, S.:
1362 Characteristics and formation of typical winter haze in Handan, one of the most
1363 polluted cities in China, *Sci. Total Environ.*, 613-614, 1367-1375,
1364 <https://doi.org/10.1016/j.scitotenv.2017.08.033>, 2018.
- 1365 [Yang, X., Wu, Q., Zhao, R., Cheng, H., He, H., Ma, Q., Wang, L., and Luo, H.: New](#)
1366 [method for evaluating winter air quality: PM_{2.5} assessment using Community](#)
1367 [Multiscale Air Quality Modeling \(CMAQ\) in Xi'an, *Atmos. Environ.*, 211, 18-28,](#)
1368 [<https://doi.org/10.1016/j.atmosenv.2019.04.019>, 2019.](#)
- 1369 Yang, X., Zhao, C., Guo, J., and Wang, Y.: Intensification of aerosol pollution associated
1370 with its feedback with surface solar radiation and winds in Beijing, *J. Geophys. Res.*
1371 *Atmos.*, 121, 4093-4099, <https://doi.org/10.1002/2015JD024645>, 2016.
- 1372 Yang, Y., Maraun, D., Ossó, A., and Tang, J.: Increased spatial extent and likelihood of
1373 compound long-duration dry and hot events in China, 1961–2014, *Nat. Hazards*
1374 *Earth Syst. Sci.*, 23, 693–709, <https://doi.org/10.5194/nhess-23-693-2023>, 2023.
- 1375 Yang, Y., and Tang, J.: Substantial Differences in Compound Long - Duration Dry and
1376 Hot Events Over China Between Transient and Stabilized Warmer Worlds at 1.5° C
1377 Global Warming, *Earths Future*, 11, e2022EF002994,
1378 <https://doi.org/10.1029/2022EF002994>, 2023.
- 1379 Yang, Y., Tang, J., Xiong, Z., Wang, S., and Yuan, J.: An intercomparison of multiple
1380 statistical downscaling methods for daily precipitation and temperature over China:
1381 future climate projections, *Clim. Dynam.*, 52, 6749–
1382 6771, <https://doi.org/10.1007/s00382-018-4543-2>, 2019.
- 1383 [Yin, Z., Wang, H., and Chen, H.: Understanding severe winter haze events in the North](#)
1384 [China Plain in 2014: roles of climate anomalies, *Atmos. Chem. Phys.*, 17, 1641–](#)
1385 [1651, <https://doi.org/10.5194/acp-17-1641-2017>, 2017.](#)
- 1386 [You, T., Wu, R., Huang, G., Fan, G.: Regional meteorological patterns for heavy](#)
1387 [pollution events in Beijing, *J. Meteorolog. Res.*, 31, 597-611,](#)
1388 [<https://doi.org/10.1007/s13351-017-6143-1>, 2017.](#)
- 1389 Yu, X., Moore, J. C., Cui, X., Rinke, A., Ji, D., Kravitz, B., and Yoon, J.: Impacts,
1390 effectiveness and regional inequalities of the GeoMIP G1 to G4 solar radiation
1391 management scenarios, *Global and Planetary Change*, 129, 10-22,
1392 <https://doi.org/10.1016/j.gloplacha.2015.02.010>, 2015.
- 1393 Zhan, P., Zhu, W., Zhang, T., Cui, X., Li, N.: Impacts of sulfate geoengineering on rice
1394 yield in China: Results from a multimodel ensemble, *Earth's Future*, 7(4), 395-410,
1395 <https://doi.org/10.1029/2018EF001094>, 2019.
- 1396 Zhang, Q., Zheng, Y., Tong, D., Shao, M., Wang, S., Zhang, Y., Xu, X., Wang, J., He, H.,
1397 Liu, W., Ding, Y., Lei, Y., Li, J., Wang, Z., Zhang, X., Wang, Y., Cheng, J., Liu, Y.,
1398 Shi, Q., Yan, L., Geng, G., Hong, C., Li, M., Liu, F., Zheng, B., Cao, J., Ding, A.,
1399 Gao, J., Fu, Q., Huo, J., Liu, B., Liu, Z., Yang, F., He, K., and Hao, J.: Drivers of
1400 improved PM_{2.5} air quality in China from 2013 to 2017, *PNAS*, 116, 24463-24469,

1401 <https://doi.org/10.1073/pnas.1907956116>, 2019.

1402 Zhang, Z., Gong, D., Mao, R., Kim, S., Xu, J., Zhao, X., and Ma, Z.: Cause and
1403 predictability for the severe haze pollution in downtown Beijing in November–
1404 December 2015, *Sci. Total Environ.*, 592, 627–638,
1405 <https://doi.org/10.1016/j.scitotenv.2017.03.009>, 2017.

1406 Zhao, D., Xin, J., Gong, C., Quan, J., Liu, G., Zhao, W., Wang, Y., Liu, Z., and Song, T.:
1407 The formation mechanism of air pollution episodes in Beijing city: insights into the
1408 measured feedback between aerosol radiative forcing and the atmospheric boundary
1409 layer stability, *Sci. Total Environ.*, 692, 371–381,
1410 <https://doi.org/10.1016/j.scitotenv.2019.07.255>, 2019.

1411 [Zheng, C., Zhao, C., Zhu, Y., Wang, Y., Shi, X., Wu, X., Chen, T., Wu, F., and Qiu, Y.:
1412 Analysis of influential factors for the relationship between PM_{2.5} and AOD in
1413 Beijing, *Atmos. Chem. Phys.*, 17, 13473–13489, \[https://doi.org/10.5194/acp-17-
13473-2017\]\(https://doi.org/10.5194/acp-17-
1414 13473-2017\), 2017.](https://doi.org/10.5194/acp-17-13473-2017)

1415 Zhou, B., Xu, Y., Wu, J., Dong, S., and Shi, Y.: Changes in temperature and precipitation
1416 extreme indices over China: analysis of a high-resolution grid dataset, *Int. J.*
1417 *Climatol.*, 36, 1051–1066, <https://doi.org/10.1002/joc.4400>, 2016.

1418 Zhu, J., Wang, S., Huang, G.: Assessing Climate Change Impacts on Human-Perceived
1419 Temperature Extremes and Underlying Uncertainties, *Journal of Geophysical*
1420 *Research: Atmosphere*, 124 (7), 3800–3821, <https://doi.org/10.1029/2018JD029444>,
1421 2019.

1422 Zhu, X., Huang, G., Zhou, X., Zheng, S.: Projection of apparent temperature using
1423 statistical downscaling approach in the Pearl River Delta, *Theor. Appl. Climatol.*,
1424 144 (3–4), 1253–1266, <https://doi.org/10.1007/s00704-021-03603-2>, 2021.

1425